PBRM1 loss in kidney cancer unbalances the proximal tubule master transcription factor hub to repress proximal tubule differentiation

Xiaorong Gu[1], Francis Enane[2], Rita Tohme[1], Caroline Schuerger[1], Tomas Radivoyevitch[3], Yvonne Parker[1], Eric Zuberi[4], Bartlomiej Przychodzen[1], Babal Kant Jha[1], Daniel Lindner[1], Brian Rini[6], Yogen Saunthararajah[1,5,7,*]

[1]Department of Translational Hematology & Oncology Research, Taussig Cancer Institute, Cleveland Clinic, Cleveland, OH, USA

[2]Indiana Center for Biomedical Innovation, Indiana University School of Medicine, Indianapolis, IN, USA

[3]Department of Quantitative Health Sciences, Cleveland Clinic, Cleveland, OH, USA

[4]Department of Biochemistry, Clemson University, Clemson, SC, USA

[5]Department of Hematology and Oncology, Taussig Cancer Institute, Cleveland Clinic, Cleveland, OH, USA

[6]Department of Hematology and Oncology, Vanderbilt University, Nashville, TN, USA

[7]Lead contact

SUMMARY

PBRM1, a subunit of the PBAF coactivator complex that transcription factors use to activate target genes, is genetically inactivated in almost all clear cell renal cell cancers (RCCs). Using unbiased proteomic analyses, we find that PAX8, a master transcription factor driver of proximal tubule epithelial fates, recruits PBRM1/PBAF. Reverse analyses of the PAX8 interactome confirm recruitment specifically of PBRM1/PBAF and not functionally similar BAF. More conspicuous in the PAX8 hub in RCC cells, however, are corepressors, which functionally oppose coactivators. Accordingly, key PAX8 target genes are repressed in RCC versus normal kidneys, with the loss of histone lysine-27 acetylation, but intact lysine-4 trimethylation, activation marks. Re-introduction of PBRM1, or depletion of opposing corepressors using siRNA or drugs, redress coregulator

imbalance and release RCC cells to terminal epithelial fates. These mechanisms thus explain RCC resemblance to the proximal tubule lineage but with suppression of the late-epithelial program that normally terminates lineage-precursor proliferation.

In brief

Gu et al. identify that transcription factor PAX8 needs the PBRM1/PBAF coactivator to activate proximal tubule genes. PBRM1 mutation/deletion thus explains the resemblance of clear cell kidney cancer to proximal tubule tissue but with suppressed terminal epithelial markers. This oncogenic mechanism could be repaired using drugs to inhibit corepressors.

Graphical Abstract
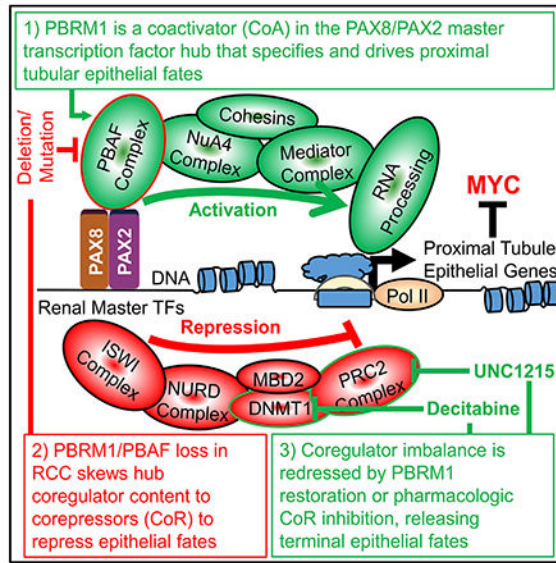
INTRODUCTION

Clear cell renal cell cancer (RCC) is the most common subtype of kidney cancer (>75% of cases). In studying RCC genesis, key observations are that the *Von Hippel-Lindau (VHL)* and *Polybromo 1* (*PBRM1*) genes have at least one allele deleted in >90% of RCC (via chromosome 3p loss), and the remaining *VHL* and *PBRM1* alleles are inactivated by mutation in ~60% and 40% of cases, respectively. *PBRM1* is thus second only to *VHL* as the most frequently inactivated gene in RCC (Cancer Genome Atlas Research Network, 2013). Underscoring the oncogenic links between PBRM1 deficiency and RCC, germline *PBRM1* loss-of-function alterations predispose specifically to RCC and not cancers of other tissues (Benusiglio et al., 2015; Bodmer et al., 1998; Li et al., 1993), and *PBRM1* deletion/mutation is >2-fold more frequent in RCC than in cancers of any other lineage (Shain and Pollack, 2013). A cause-effect relationship has been verified in murine models: deletion of *Pbrm1* and *Vhl* from murine kidney using *Ksp-Cre* produced RCC in 33% of mice (deletion of either *Pbrm1* or *Vhl* alone did not produce RCC) (Nargund et al., 2017). Further, using *paired box 8 (Pax8)-Cre* instead of *Ksp-Cre* to effect proximal tubule

lineage-specific deletion of *Pbrml* and *Vhl* produced large RCCs with 100% penetrance (Gu et al., 2017): Pax8 is a master transcription factor essential for kidney proximal tubular epithelial fates; humans with germline *PAX8* mutations have congenital kidney defects, *Pax8* knockout mice have abnormal kidney ontogeny, and Pax8 has been biochemically verified to regulate key kidney epithelial genes (Barr et al., 2015; Boualia et al., 2013; Bouchard et al., 2002; Buisson et al., 2015; Carvalho et al., 2013; Dehbi and Pelletier, 1996; di Gennaro et al., 2013; Di Palma et al., 2013; Fraizer et al., 1997; Green et al., 2009; Grote et al., 2006; Meeus et al., 2004; Narlis et al., 2007; Ribes et al., 2003; reviewed in Boualia et al., 2013). Consistent with the transformation of the PAX8-dependent proximal tubular lineage, human RCC pheno-copies kidney proximal tubular epithelium but with loss of expression of terminal epithelial differentiation markers (Ebert et al., 1990; Holthöfer et al., 1983; Klingel et al., 1992), and in fact, PAX8 is a dependency of human RCC cells–RCC cells cease to exist upon PAX8 knock down (Bleu et al., 2019; Li et al., 2011; McDonald et al., 2017; Tsherniak et al., 2017). It is still not known, however, how PBRM1 deficiency transforms the proximal tubular lineage, and there are no treatments to correct these unknown mechanisms.

The biochemical function of PBRM1, however, is known: PBRM1 is a subunit of the PBAF multi-protein coactivator complex. That is, transcription factors recruit and use PBAF to remodel chromatin for gene activation (Hartley and Madhani, 2009; Lemon et al., 2001; Parnell et al., 2008). Specifically, once recruited to specific gene loci by transcription factors, PBRM1/PBAF uses the energy from ATP hydrolysis to mobilize and reposition histones, creating nucleosome-free regions around transcription start sites that can accommodate the large macromolecular machinery that transcribes genes (basal transcription factor complex, RNA polymerase, etc.) (Barisic et al., 2019; Hartley and Madhani, 2009; Lemon et al., 2001; Parnell et al., 2008). PBRM1 contains six bromodomains that bind acetylated lysines on histones, e.g., histone lysine 27 acetylation (H3K27ac), a histone modification linked to gene activation. PBRM1 is the protein module that distinguishes the PBAF coactivator complex from BAF, the other major nucleosome repositioning ATPase coactivator complex in cells. Transcription factors are particular in their coactivator usage to the extent of discriminating even between closely similar PBAF and BAF (Kadam and Emerson, 2003; Kadam et al., 2000; Lemon et al., 2001; Sikorski et al., 2012). Thus, toward understanding the cellular fate/function consequences of PBRM1 loss in RCCs, we first sought to identify the transcription factors that direct PBRM1/ PBAF function in kidney cells. We did this using unbiased immunoprecipitation and liquid chromatography-tandem mass spectrometry (IP-LCMS/MS) analyses of the endogenous PBRM1 interactome in non-malignant kidney and RCC cells. Most abundant and notable of the transcription factors found was PAX8. Reverse characterization of the endogenous PAX8 hub confirmed the PAX8 interaction with PBRM1 and other PBAF protein modules but not with BAF-specific components such as ARID1A or ARID1B. Even more abundant in the PAX8 protein hub in RCC cells, however, were corepressors. Corepressors oppose coactivators by remodeling chromatin to repress rather than activate gene transcription. This mechanism connects PBRM1 loss, the 2nd most recurrent genetic alteration in RCC, to RCC pathobiology; it has a resemblance to the kidney proximal tubule lineage but with a loss of expression of terminal epithelial differentiation markers. This oncogenic

mechanism could be countered, including by clinically viable intervention distinct from present treatments: PBRM1 re-introduction, or depleting corepressors from the PAX8 hub using siRNA or clinical small molecules, physically and functionally re-equilibrating the PAX8 master transcription factor hub toward coactivators and thereby releasing terminal epithelial differentiation as expected from RCC PAX8 content.

RESULTS

The endogenous PBRM1 protein interactome in non-malignant and malignant kidney cells

Endogenous PBRM1 was immunoprecipitated from non-malignant kidney cells (human embryonic kidney cells, HEK293) and RCC cells that contained an inactivating mutation in *PBRM1* (ACHN), and co-purified proteins were analyzed by IP-LCMS/MS. As expected, subunits of the PBAF coactivator complex (SMARCA4, SMARCC1, SMARCC2, BRD7, and ARID2) were the most abundant proteins in the PBRM1 protein interactomes from both the non-malignant and malignant cells (p value Bonferroni-corrected $< 1.42 \times 10^{-27}$) Figure 1; Table S1). Protein subunits specific to the BAF coactivator complex, ARID1A and ARID1B, were not detected (Figures 1A and 1B; Table S1). Three transcription factors were found in substantial amounts in the PBRM1 interactomes from both cell types: PAX8, GA-binding protein transcription factor alpha subunit (GABPA), and translin (TSN) (Figures 1A and 1B; Table S1); of these, PAX8 was the transcription factor most abundantly represented in the PBRM1 interactome in RCC cells (Figures 1A and 1B; Table S1). PBRM1/PAX8 interactions observed by immunoprecipitation (IP) and LCMS/MS were extended and corroborated by bi-directional IP-western blots in ACHN and two additional RCC cell lines (SKRC45 and SKRC29) and in HEK293 non-malignant kidney epithelial lineage cells (Figure 1C). Other kidney proximal tubule transcription factors that are also highly expressed in RCC cells, at levels similar to PAX8, were not detected in the PBRM1 interactome (Figures 1A and 1B; Table S1).

Composition of the PAX8 master transcription factor hub in RCC cells

We then performed the reverse proteomic interrogation, immuno-precipitating endogenous PAX8 from two RCC cell lines (SKRC-45 with one allele of *PBRM1* deleted and ACHN with one allele of *PBRM1* mutated), followed by LCMS/MS to catalog proteins copurifying with PAX8. We focused on PAX8 since (1) it was the transcription factor found in the greatest abundance in the PBRM1 pull-down; (2) PAX8 is a master transcription factor driver of kidney epithelial-fates (reviewed in Boualia et al., 2013), and (3) GABPA and TSN are ubiquitously expressed transcription factors with protean functions in mitochondrial maintenance and proliferation, respectively (Agrawal et al., 2010; Wu et al., 2013; Yang et al., 2004), and were therefore less likely to explain the proximal tubule lineage-specific transformation observed with germline PBRM1 deficiency (Benusiglio et al., 2015; Bodmer et al., 1998; Li et al., 1993). In both RCC cell lines, the endogenous PAX8 hub contained PAX2 and GATA3, master transcription factors known to collaborate with PAX8 to drive kidney lineage fates (Boualia et al., 2013) (Figures 2A and 2B; Table S2). Also present in high amounts were PBRM1 and other protein modules of the PBAF coactivator complex (Figures 2A and 2B), as were coactivators KMT2A (MLL1) and KMT2B (MLL2) of the tri-thorax family of coactivators and the NUA4 coactivator complex that contains

histone acetyltransferase function (RUVBL1, RUVBL2, EPC1, EP300, TIP60, TRRAP, TADA2B) (Figures 2A and 2B; Table S2). By contrast, components specific to the BAF coactivator complex, ARID1A nor ARID1B, were not detected (Figures 2A and 2B). Even more conspicuous and abundant in the RCC cell PAX8 interactomes than the coactivators were corepressors that oppose coactivators to repress genes, which included DNA methyltransferase 1 (DNMT1), the NURD complex, NCoR/SMRT complex, SIN3A complex, and ISWI (SMARCA5) (relative enrichment p value Bonferroni-corrected 3.47×10^{-29}) (Figures 2A and 2B; Table S2).

Components of the PBRM1/PBAF coactivator recruited by PAX8 are recurrently deleted/ mutated in RCC, while druggable corepressors recruited by PAX8 are recurrently amplified

Genes for several components of the PBRM1/PBAF coactivator recruited by PAX8 (*PBRM1*, *SMARCC1*, *SMARCA2*) were recurrently deleted and mutated at a high rate in RCCs (Figures 3A and 3B) (n = 342, TCGA; Cancer Genome Atlas Research Network, 2013). These deletions/inactivating mutations impacted expression: PBRM1/ PBAF coactivator component expression was lower in RCCs with the deletion of one allele and lowest in RCCs with the deletion/mutation of both alleles versus RCCs with intact coactivator genes or compared to normal kidney (Figure 3C). On the other hand, genes for druggable components of corepressor complexes recruited by PAX8 (*EZH2*, *CHD4*, *DNMT1*) were frequently gained or amplified in RCCs (Figure 3B). These gain/amplifications increased corepressor component expression: for two of these three corepressor components, gene expression was significantly higher in RCCs with copy-number gains/amplifications than RCCs without (Figure 3D).

The epithelial program downstream of PAX8/PAX2 is repressed in RCC

Enrichment for corepressors over coactivators in the PAX8 transcription factor hub in RCC cells suggested key PAX8 target genes might be repressed instead of activated. Key PAX8 target genes, identified by several groups, are the transcription factors GATA binding protein 3 (*GATA3*), LIM homeobox protein 1 (*LHX1*), and Wilms tumor 1 (*WT1*) that, together with PAX8 and PAX2, form a core transcription factor circuit that drives to proximal tubular epithelial fates (reviewed in Boualia et al., 2013) (Figure 4A). Consistent with these other reports, we found by chromatin IP (ChIP)-qRT-PCR analyses that endogenous PAX8 localized at *GATA3*, *LHX1*, and *WT1* regulatory elements in RCC cells (Figure 4B). In public datasets of ChIP-sequencing (ChIP-seq) data, the histone modifications linked to gene activation, H3K27ac and H3K4me3 were created at *PAX8*, *PAX2*, *GATA3*, *LHX1* and *WT1* in normal kidney compared to embryonic stem cells (ESCs) (Figure 4C); this same remodeling for activation occurred at *PAX8* and *PAX2* in RCC cells (CAKI1) but not at the PAX8/PAX2 target genes *GATA3*, *LHX1* and *WT1*, at which remodeling to create H3K27ac did not occur, even though the H3K4me3 mark was generated as in normal kidney (Figure 4C). Accordingly, *PAX8*/*PAX2* was activated to similar levels in RCCs and the normal kidney cortex (there was a small decrease in PAX8 expression consistent with its known autoregulation of its expression (reviewed in Boualia et al., 2013), but *GATA3*, *LHX1*, and *WT1* expression were as much as 30-fold lower in RCCs (Figure 4D) (TCGA gene expression), with the greatest suppression in RCCs containing bi-allelic versus uni-allelic *PBRM1* inactivation (Figure 4D) (also seen in paired analyses grouped by tumor size and

invasiveness; Figure S1). We also examined the CpG methylation repression mark: CpG methylation levels at *PAX8/PAX2* were similar in the normal kidney cortex and RCCs but was several-fold increased at *GATA3*, *LHX1*, and *WT1* gene loci in RCCs, again to the greatest extent in RCCs with bi-allelic *PBRM1* inactivation (Figure 4E).

This disruption to the core transcription factor circuit suggested that hundreds of downstream proximal tubule genes would also be suppressed. Genes enriched specifically in normal proximal tubules versus other normal human tissues were identified from databases of kidney development (Brunskill et al., 2008) and normal tissue expression (Ge et al., 2005; Lindgren et al., 2017) (~1,500 genes) (Table S3). More than 1,000 of these genes were significantly repressed in RCCs versus the normal kidney cortex, in a consistent pattern across >500 RCC samples versus >70 normal controls (Figure 4F; Table S3) (TCGA RNA sequencing [RNA-seq]). Again, there was a specific failure to create the H3K27ac activation mark at these ~1,000 suppressed genes, even as the H3K4me3 activation mark was normally generated (Figure 4G); nucleosome positions also appeared more compressed around transcription start sites, interpreted from locations of H3K27ac and H3K4me3 signal peaks (Figure 4G). Larger and more locally invasive tumors were characterized by a greater suppression of the proximal-tubule/kidney-epithelial program (Figure S2A) and worse corepressor/coactivator imbalance: more deletions of PBAF coactivator components *PBRM1*, *SMARCA2*, and *SMARCC1*, and more gains in corepressor components *EZH2*, *CHD4*, and *DNMT1* (Figures S2B and S2C).

These observations were corroborated by unbiased identification of gene expression programs repressed in RCCs versus the normal kidney cortex: we used unsupervised hierarchical clustering and marker selection (Morpheus, Broad Institute) to identify ~2,700 genes that were significantly less or more expressed (RCC n = 533; normal kidney cortex n = 72; TCGA RNA-seq data [Cancer Genome Atlas Research Network, 2013]). Of the ~1,300 most suppressed genes in RCCs versus the normal kidney, 42% were categorized by Gene Ontology analyses as kidney differentiation genes (DAVID; Huang et al., 2009), with specialized kidney epithelial functions in cation transport, cell adhesion, and cell excretion (Brunskill et al., 2008) Figure S2D; Table S4), and none were "cancer" genes with functions in cell division and signal transduction (Figure S2D). The opposite was true of the ~1300 genes most expressed in RCCs versus the normal kidney cortex: none were kidney differentiation genes while 25% were "cancer" genes (Figure S2D; Table S4). Thus, unbiased analyses also indicated kidney epithelial differentiation genes as the most prominently suppressed genes in RCCs versus the normal kidney cortex.

PBRM1 re-introduction physically and functionally reconfigured the PAX8 hub to coactivators

We then examined the effects of PBRM1 restoration on the PAX8 master transcription factor hub. PBRM1 (FLAG-tagged) was introduced into *PBRM1*-mutated RCC cells (ACHN) by transfection with an expression vector (Figure 5A). Western blots for FLAG and PBRM1 in PBRM1 versus empty-vector-transfected cells indicated that introduced PBRM1 levels were in a physiologically relevant range (Figure 5B). The endogenous PAX8 protein was then immunoprecipitated from these cells, and the interactome was analyzed by LCMS/MS

and western blot. PBRM1 introduction produced a substantial shift from corepressors to coactivators in the PAX8 protein interactome by LCMS/MS analyses (Figures 5C and 5D; Table S5). This was also seen in western blot analyses that focused on PBRM1 (Figure 5B). The gene expression and cell fate consequences of this shift in coregulator content of the PAX8 hub were then examined. PBRM1 transfection activated the PAX8 target genes *GATA3*, *WT1*, and *HNF4A* by >2-fold (*LHX1* was not upregulated) (Figure S3A); decreased protein levels of MYC the master oncoprotein transcription factor driver of cell growth and division (Figure S3B); increased protein levels of p27/CDKN1B the canonical cyclin-dependent kinase inhibitor that mediates cell cycle exits by terminal epithelial-differentiation (Figure S3B); induced cell morphology changes consistent with epithelial differentiation by Giemsa-staining (decrease in nuclear-cytoplasmic ratio) and by flow cytometric analyses (increase in side-scatter) (Figures S3C and S3D); and decreased proliferation of the RCC cells (Figure S3E).

Depleting or inhibiting corepressors also restored PAX8 hub transactivating function

We then examined if depletion or inhibition of corepressors could also rebalance the PAX8 transcription factor hub toward target gene activation. DNMT1 is the maintenance methyltransferase and also a corepressor recruited by PAX8 (Figure 2). We used siRNA to knock down DNMT1 from RENO1 and SKRC29 RCC cells (Figure S4A): knock down was confirmed by western blot for DNMT1 in siDNMT1 transfected cells compared to parental RCC cells and RCC cells transfected with scrambled siRNA (Figure S4B). The DNMT1 knock down activated by several-fold the key PAX8 target genes *GATA3*, *WT1*, and *HNF4A* (that were also activated by PBRM1 re-introduction) (Figure S4C), accompanied by cell morphology changes of epithelial differentiation by morphology and flow cytometry (decrease in nuclear cytoplasmic ratio, increase in side- and forward-scatter) (Figure S4D), and decreased proliferation of the siDNMT1-transfected, but not parental- or scrambled siRNA-transfected, RCC cells (Figure S4E).

DNMT1 can also be depleted from cells by non-cytotoxic concentrations of the clinical compound decitabine. We treated RCC cells (SKRC-45) with vehicle versus decitabine 0.5 µM (a concentration that depletes DNMT1 from RCC cells without cytotoxicity [Negrotto et al., 2011]) then immunoprecipitated endogenous PAX8 and analyzed the interactome by LCMS/MS and western blot (Figure 6A). DNMT1 depletion by decitabine shifted the composition of the PAX8 master transcription factor hub from corepressors to coactivators, seen both by LCMS/MS (Figures 6B and 6C; Table S6) and western blot (Figure 6D). As an additional control, we included a conventional cytotoxic drug, camptothecin, at 10 µM; this did not produce a similar shift from corepressors to coactivators (Figure 6D). The shift produced by decitabine was accompanied by activation of *GATA3*, *LHX1*, *HNF4A*, and *WT1* by several-fold (Figures 7A and 7B), decreased protein levels of MYC (Figure 7C), increased protein levels of p27/CDKN1B (Figure 7C), induced morphology changes consistent with epithelial differentiation (decrease in nuclear/cytoplasmic ratio) (Figure 7D), and substantially decreased proliferation of RCC cells (ACHN, SKRC-45) (Figure 7E). L3MBTL3 is another corepressor in the PAX8 interactome for which there is an available non-cytotoxic small molecule inhibitor (UNC1215, which inhibits the methylated lysine reading function of L3MBTL3 [IC$_{50}$ 40 nM] for L3MBTL3). Non-cytotoxic concentrations

of UNC1215 (1 μM) also activated *GATA3*, *WT1*, and *HNF4A*, downregulated protein levels of MYC, upregulated protein levels of p27/CDKN1B, induced morphologic changes of epithelial differentiation, and decreased proliferation in RCC cells (ACHN, SKRC-45), although not to the same extent as DNMT1 depletion by decitabine (Figure 7).

Since decitabine is a compound available for *in vivo*/clinical use, we also evaluated decitabine *in vivo*, alone and in combination with an inhibitor, tetrahydrouridine, of the enzyme cytidine deaminase that otherwise rapidly inactivates decitabine *in vivo* (Negrotto et al., 2011) (Figure S5). RCC cells were injected into both flanks of nude mice and, treatment with vehicle, sunitinib (standard clinical treatment positive control), decitabine, or tetrahydrouridine-decitabine was initiated on day seven, when tumor diameter was >5 mm (n = 8/group). Treatment was continued until day thirty-three, when the experiment was terminated for tumor size exceeding >17 mm in diameter in the vehicle-treated mice (Figure S5A). Tetrahydrouridine-decitabine produced the greatest tumor regression, to unmeasurable amounts, in several mice (Figure S5A). Where still present, the tumor was resected and analyzed by western blot. The DNMT1 protein was depleted from the tumor by both decitabine and tetrahydrouridine-decitabine (more by tetrahydrouridine-decitabine), while tetrahydrouridine-decitabine produced the greatest reductions in MYC and the greatest increases in p27/CDKN1B (Figure S5B).

Baseline differences in H3K27ac amounts at housekeeping/proliferation versus epithelial genes

RCC cells activate housekeeping genes (3,804 genes identified by consistent expression across tissues [Eisenberg and Levanon, 2013]) and MYC-target (proliferation genes, 356 genes identified by ChIP analyses [Kim et al., 2010]) to levels similar to that observed in normal kidney cortex, even as the PAX8 target epithelial-differentiation program is simultaneously repressed (Figure S6A; Table S7). This selective repression occurred even though GABPA and TSN, with housekeeping functions, also recruited PBRM1 (Figure 2). One potential explanation for this selective repression of epithelial differentiation but not housekeeping/proliferation is a difference in baseline chromatin configuration and hence remodeling work needed for activation. H3K27ac amounts at housekeeping/proliferation genes were similarly high in ESCs (the ultimate baseline), normal kidney cells, and RCC cells (Figure S6B). By contrast, H3K27ac at proximal-tubule/kidneyepithelial genes was low to begin with in ESCs and substantially increased in normal kidney, but this increase failed to occur in RCCs (Figure S6B). A difference in chromatin remodeling needed for activation may thus contribute to epithelial-program-selective consequences of PBRM1/PBAF loss.

DISCUSSION

The PBRM1/PBAF coactivator complex is directed to gene loci by transcription factors. Thus, to identify the pathways by which PBRM1 loss-of-function contributes to RCC genesis, we looked for transcription factors that direct PBRM1/PBAF function. Unbiased proteomic analyses of the endogenous PBRM1 interactome in kidney lineage cells identified PAX8, a master transcription factor essential for proximal tubular epithelial fates. The reverse proteomic analysis of the endogenous PAX8 interactome confirmed PAX8

recruitment of PBRM1/PBAF but not the related BAF coactivator complex. PBRM1 loss in RCC cells skewed coregulator composition of the PAX8 master transcription factor hub toward corepressors that repress rather than activate target genes. This consequence was documented; *PAX8* and its collaborator *PAX2* were similarly activated in RCCs versus the normal kidney cortex, but their key target genes, such as *GATA3*, *LHX1*, *WT1*, and >1,000 other kidney epithelial genes, were substantially repressed in RCCs, with a significantly lower H3K27ac activation mark and a significantly higher CpG methylation repression mark but preserved H3K4me3 activation mark, changes that were most prominent in RCC cases with bi-allelic *PBRM1* inactivation. As a potential explanation for the selective loss of H3K27ac but not H3K4me3, PBRM1/PBAF binds to H3K27ac, an action that may help anchor other coactivator complexes, e.g., NuA4, that may contain the histone acetyltransferase activity needed to propagate H3K27ac; PBRM1/PBAF has no components/ domains with H3K4me3 reader or writing function (Eberl et al., 2013). PAX8 reliance on PBRM1/PBAF to activate its proximal tubule epithelial differentiation target program can also explain why germline mutation or deletion of *PBRM1* predisposes specifically to RCC, a cancer of the PAX8-dependent proximal tubule lineage, and not cancers of other tissue lineages (Benusiglio et al., 2015; Bodmer et al., 1998; Li et al., 1993) and why somatic *PBRM1* inactivating mutations are >2-fold higher in RCCs (~40%) versus cancers of other lineages (<20%) (Shain and Pollack, 2013). Corroborating observations from others support these conclusions: (1) *Paired box 8 (Pax8)-Cre-mediated* deletion of *Pbrm1* and *Vhl* produced large RCCs with 100% penetrance (Gu et al., 2017), demonstrating a critical role for Pbrm1 and Vhl for Pax8-dependent lineage-maturation; (2) lower PBRM1 protein expression in RCCs is linked with greater disruption to proximal tubule differentiation by pathologic criteria, as well as worse overall survival (Jiang et al., 2017; Pawłowski et al., 2013); (3) CpG hypermethylation in RCCs is observed specifically at promoters and enhancers of kidney epithelial-differentiation genes (Cooper et al., 2010; Ellinger et al., 2010; Ho et al., 2016; Hu et al., 2014; Kanao et al., 2008; Minardi et al., 2009; Mosashvilli et al., 2010; Tun et al., 2010); and (4) there is an overall decrease in chromatin modifications linked to gene activation, e.g., H3 acetylation, in RCCs (Cooper et al., 2010; Hu et al., 2014; Minardi et al., 2009; Tun et al., 2010). Others have also found that the loss of a single protein module can disrupt multi-protein coactivator complexes, shown for the mediator coactivator complex (Marr et al., 2006), and that coactivator/corepressor stoichiometry impacts transcription activation (Chronis et al., 2017; Dannenberg et al., 2005; Enane et al., 2017a; Gu et al., 2014; Hu et al., 2011; Linderson et al., 2004; Perissi et al., 2010; Ram et al., 2011; Rosenfeld et al., 2006; Sen et al., 2017; Söderström et al., 1997; Wang et al., 2009; Zamir et al., 1997).

Re-introducing PBRM1 into PBRM1-deficient RCC cells physically re-equilibrated the PAX8 interactome toward coactivators, activated proximal tubule differentiation genes, decreased MYC protein levels, increased p27/CDKN1B, produced cell morphology consistent with epithelial-differentiation, and terminated proliferation, which are outcomes expected from baseline-high PAX8 expression in RCCs, its localization at key PAX8 target genes, and an overall gene expression pattern and phenotype of RCC cells that indicates at least partial maturation within the proximal tubule lineage to begin with. These biochemical and cell-fate outcomes were also produced, *in vitro* and *in vivo*, by knock down of the

corepressor DNMT1 from the PAX8 hub using siRNA or a clinical drug decitabine (we also previously showed decitabine-mediated restoration of RCC epithelial-differentiation [Negrotto et al., 2011]). Cell-cycle exits via epithelial differentiation do not require the p53/p16-apoptosis axis (Negrotto et al., 2011; Saunthararajah et al., 2015; Velcheti et al., 2017). Hence, remedying corepressor/coactivator imbalance by pharmacologic targeting of specific corepressors can be a treatment modality distinct from conventional p53/p16/apoptosis-based therapies that are inadequate for RCCs containing p53 or p16/CDKN2A deletions (~30% of patients) (Heng et al., 2013).

Loss of *Vhl* (the most commonly inactivated gene in RCCs) or *Pbrm1* (the 2nd most commonly inactivated gene in RCC) alone did not cause RCC in mice, but the loss of both produced RCC with high penetrance (Gu et al., 2017; Nargund et al., 2017). The present observations provide a model for such collaboration: *VHL* loss stabilizes MYC, the master transcription factor regulator of cell proliferation, in a transcriptionally active form (Dang et al., 2008; Shuib et al., 2011). MYC is nevertheless subordinate to and antagonized by key epithelial differentiation driving factors, e.g., GATA3, WT1, and p27/CDKN1B, that are downstream of PAX8 (Acosta et al., 2008; Aschauer et al., 2013; Green et al., 2009; Grote et al., 2006; Kojima et al., 2010; Lucas et al., 2005; Negrotto et al., 2011; Ramaswamy et al., 2002). In other words, persistent MYC-driven proliferation requires not just VHL loss to stabilize MYC but also PBRM1/PBAF deficiency to repress the epithelial-differentiation program that otherwise dominantly antagonizes MYC to terminate proliferation (Chowdhury et al., 2016). Neoplastic evolution builds on dual *VHL/PBRM1* haploinsufficiency created by chromosome 3p deletion by inactivating additional PBAF components, e.g., *SMARCA2*, and by amplifying corepressors recruited by PAX8, e.g., *CHD4*, to thereby worsen PAX8 hub corepressor/coactivator imbalance and resulting friction to lineage maturation.

Why is *PBRM1* mutated instead of *PAX8* directly? PAX8 is a dependency of proximal tubule lineage cells, and PAX8 knock down eliminates RCC cells; RCC cells, which are of the proximal tubule lineage, require PAX8 to exist (Li et al., 2011; McDonald et al., 2017; Tsherniak et al., 2017). *PBRM1* loss, on the other hand, disrupts PAX8-mediated activation of the terminal epithelial program, which requires substantial chromatin remodeling for activation, but meanwhile preserves activation of housekeeping/proliferation genes that have constitutively high H3K27ac and thus do not require extensive chromatin remodeling for activation. This oncogenic motif of corepressor/coactivator imbalance to decouple lineage-maturation and proliferation is observed in cancers of other lineages also (Enane et al., 2017a; Gu et al., 2014, 2018; reviewed in Velcheti et al., 2018).

In sum, PBRM1 coactivator loss in RCCs skews coregulator content in the PAX8 kidney lineage master transcription factor hub toward corepressors, to thereby repress the terminal proximal tubule epithelial program. This mechanism connects PBRM1 loss, the 2nd most recurrent genetic alteration in RCCs, to RCC pathobiology by its resemblance to the kidney proximal tubule lineage but with loss of expression of terminal epithelial differentiation markers. This oncogenic mechanism can be countered: inhibiting corepressors with small molecule drugs rebalances to PAX8 hub transactivating function to activate terminal epithelial fates. This candidate therapeutic modality for RCC cell-cycle exits does not rely on the p53/p16/apoptosis-system that mediates conventional chemoradiation.

STAR★METHODS

RESOURCE AVAILABILITY

Lead contact—Further information and requests for resources and reagents should be directed to and will be fulfilled by the lead contact, Yogen Saunthararajah (saunthy@ccf.org).

Materials availability—Further information and requests for resources and reagents should be directed to Xiaorong Gu (gux@ccf.org).

Data and code availability—The mass spectrometry proteomics data have been deposited to the ProteomeXchange Consortium (http://proteomecentral.proteomexchange.org) with the dataset identifier: PXD020544.

This paper does not report original code.

Any additional information required to reanalyze the data reported in this paper is available from the lead contact upon request.

EXPERIMENTAL MODEL AND SUBJECT DETAILS

Animals—8-12 weeks old male outbred homozygous athymic nude mice ($Foxn1^{nu}$/$Foxn1^{nu}$) (Jackson Laboratories, Bar Harbor, ME) were used in the study. All animal studies were conducted according to the "Principles of Laboratory Animal Care" (NIH publication No. 85023, revised 1985) and approved by the Cleveland Clinic Institution Animal Care and Use Committee (IACUC)(protocol number 2464).

Cell lines—Human RCC cell line ACHN was initiated from the malignant pleural effusion of a male with widely metastatic renal adenocarcinoma. These cells were a gift from Bauer et al. (2003). SKRC45 was initiated from RCC cells metastatic to an adrenal gland in a male with RCC, and SKRC29 was initiated from RCC metastatic to the ovaries of a female with RCC; both of these cell lines were a gift from Dr N.H. Banker at The New York Hospital-Cornell Medical Center (Ebert et al., 1990). The 293T cell line is derived from human embryonic kidney cells (HEK293) transfected with a plasmid encoding a temperature-sensitive mutant of the SV40 large T antigen. These cells were purchased from ATCC, Washington DC, DC. The RCC and 293T cells were cultured in Dulbecco's Modified Eagle medium (DMEM) with 10% fetal bovine serum (FBS), 100U ml^{-1} penicillin and 100 μg ml^{-1} streptomycin (Mediatech, Herndon, VA).

METHOD DETAILS

***In vitro* treatment of cells with DNMT1 inhibitor or L3MBT2/3L inhibitor**—DNMT1 inhibitor, Decitabine, stock solution (5 mM) was generated by reconstituting lypholized decitabine (Tocris, Cat# 2624) in 100% DMSO. L3MBT2/3L inhibitor (UNC1215) was obtained from Structural Genomics Consortium and reconstituted to 10mM stock solution with 100% DMSO. Working solution was generated by diluting the stock solution 1:10 in ethanol immediately before addition to the cells, followed with a further 1:1000 dilution to the cell culture to reach the final 0.5 μM concentration for Decitabine or 1

μM L3MBT2/3L inhibitor (UNC1215). Equal amounts of ethanol and DMSO were added to the cell culture as the vehicle control. Cells were treated on day 1, 2 and 3 per week.

Giemsa staining of cells—Cytospins of cells from bone marrow or peripheral blood were fixed for 2 minutes in methanol, air-dried, and stained for 20 minutes with filtered modified solution of Giemsa stain (Sigma Aldrich, Cat # 48900, St Louis, MO), diluted (1:20) with buffer solution pH6.5, rinsed with distilled water, air-dried and examined using low and high magnifications with a Leica DMR microscope (Leica Microsystems, Wetzlar GmbH, Germany) connected to Nuance multispectral imaging system FX using Nuance version 3.0.2 software (PerknElmer, Inc., Hopkinton, MA)

PBRM1 transfection—WT PBRM1 cDNA was cloned into 3x-p-Flag-CMV4 (Cyagen Vectorbuilder, Santa Clara, CA). Sequence confirmation of flag-tagged wild-type PBRM1 was performed using Dideoxy Sanger sequencing with CMV promoter primers. Transient transfection of PBRM1 WT or Empty Vector control into RCC cells was performed using transfection polymer xfect (clonetech, Mountain view, CA). Cell pellets were isolated at 0, 48, 72 and 96 hours after transfection for downstream analysis. Cell proliferation was measured by automated cell counter.

Chromatin immunoprecipitation (ChIP)—Crosslinking to generate protein-DNA complexes was by incubating the cells (~20 million) with 1% Formaldehyde for 10 minutes at room temperature. The reaction was quenched by adding 1M Glycine to a final concentration of 125 mM for 5 minutes at room temperature. Cells were pelleted and the supernatant was removed. Cell pellets were resuspended in 1mL CHIP lysis buffer (Millipore, Cat # 17-295) with protease inhibitors, and sonicated to shear DNA to an average fragment size of 200 –500 bp, followed by centrifugation at 8000 g for 5 min to pellet the cell debris. The supernatant was transferred to a clean tube, diluted 10 times with CHIP dilution buffer (Millipore, Cat # 20-153) with protease inhibitors, and precleaned with Protein A agarose/Salmon Sperm DNA (Millipore, Cat # 16-157) for 1 hour at room temperature. The cleaned supernatant was then incubated with Mouse anti-PAX8 (SCBT, sc-81353) and normal mouse IgG ((SCBT, sc-2025) overnight at 4° C. Protein A agarose/ Salmon Sperm DNA (Millipore, Cat # 16-157) was added and incubated for another 1 hour at room temperature. The mixture was centrifuged at for 2 min at 500 g and the supernatant was removed. The beads were washed once with 1 mL Low Salt Immune Complex Wash Buffer (Millipore, Cat # 20-154), once with 1 mL High Salt Immune Complex Wash Buffer (Millipore, Cat #20-155), once with 1 mL LiCl Immune Complex Wash Buffer (Millipore, Cat # 20-156), and twice with 1mL TE Buffer (Millipore, Cat # 20-157). Protein/DNA complexes bound beads were incubated with 100 μL of elution buffer containing 1%SDS, 50mM NaHCO$_3$for 15 min at 37°C. The process was repeated twice with additional 50 μL of elution buffer. Elutes were combined. To reverse crosslinks of protein/DNA complexes, 8 μL of 5M NaCl was added to every 200 μL of elutes and incubated at 65°C for 8-10 hours or overnight followed by adding 1 μL of RNase A and incubated for 30 min at 37°C. Excess protein products were cleaned with proteinase K. The enriched fragment DNA products were purified with ChIP DNA Purification Kit (Active Motif, Cat # 58002).

RNA isolation—Total RNA from cultured cells was isolated using NucleoSpin® RNA (Clontech, Cat# 740984.5) according to the manufacturer's instruction. The cDNA was then synthesized from total RNA using the iScript cDNA synthesis Kit (BioRad, Cat# 1708891).

Reverse transcription (RT) and real-time PCR—Quantitative gene expression levels were detected using real-time PCR with the ABI PRISM 7500 Fast Sequence Detection System and SYBR Advantage qPCR Premix (Clontech, 639676) according to the manufacturer's instructions. Primers for all genes analyzed were purchased from Integrated DNA Technologies. Please see STAR Methods for Primer sequences. The relative number of copies of mRNA (RQ) was calculated based on the average C_t values using the housekeeping gene GAPDH as internal control and vehicle-treated cells as biological controls. Results are shown as mean ± SD of three independent experiments.

Covalent binding of antibody to protein G beads for immunoprecipitation—Rabbit anti-PBRM1 (Bethyl Lab, A301-590A), mouse anti-PAX8 (SCBT, sc-81353) and control IgG were covalently coupled to Sepharose-protein A/G (SCBT, sc-2003) beads using dimethylpimelimidate (Sigma-Aldrich, D8388). Briefly, 200 μL of Sepharose-protein A/G was washed with 1x PBS twice, incubated with 200 μL of antibody (20 μg) solution (1X PBS) for 1 hour at room temperature. Antibody bound protein A/G beads were then incubated with 1% chicken egg ovalbumin in PBS for another hour to block nonspecific binding sites. After 3 washes with 1X PBS, 25 mg of dimethylpimelimidate in 1 mL of 200mM triethanyl amine was added, and coupling reaction was proceeded at room temperature for 30 minutes. The reaction was repeated 2 more times with fresh addition of dimethylpimelimidate and quenched with 50mM ethanolamine. The reacted protein A/G beads were washed extensively with 1X PBS before immunoprecipitation.

Immunoprecipitation—Nuclear protein extracts (~10 mg of protein) were transferred to tubes with antibody-bound protein A/G beads and rocked gently at 4°C overnight. Nonspecifically bound proteins were removed with 5 washes of $1 \times$ PBS containing 1% Nonidet P-40. Immunoprecipitation products were extracted from protein G beads using Laemmli sample buffer.

NanoLC-ESI-LTQ-Orbitrap MS/MS—Immunoprecipitation products were subjected to SDS-polyacrylamide gel electrophoresis and stained with colloidal Coomassie Blue (Gel Code Blue, Pierce Chemical). Gel slices were excised from the top to the bottom of the lane; proteins were reduced with dithiothreitol (Sigma-Aldrich, D0632, 10mM), alkylated with iodoacetamide (Sigma-Aldrich, I1149, 55mM), and digested *in situ* with trypsin. Peptides were extracted from gel pieces 3 times using 60% acetonitrile and 0.1% formic acid/water. The dried tryptic peptide mixture was redissolved in 20 μL of 1% formic acid for mass spectrometric analysis. The LC-MS system, ThermoScientific Fusion Lumos mass spectrometer interfaced with dionex Ultimate 3000 UHPLC with Dionex column (15 cm × 75 mm id Acclaim Pepmap C18, 2 μm, 100 Å reversed- phase capillary chromatography column) were used for data collection. The extracts from trypsin digest (5 μL) were injected and the peptides eluted using acetonitrile and 0.1% formic acid gradient at a flow rate of 0.3 μL/min. The microelectrospray ion source is operated at 1.9 kV.

Database search and data validation—Mascot Daemon software (version 2.3.2; Matrix Science, London, UK) was used to perform database searches, using the Extract_msn.exe macro provided with Xcalibur (version 2.0 SR2; Thermo Fisher Scientific) to generate peaklists. The following parameters were set for creation of the peaklists: parent ions in the mass range 400–4500, no grouping of MS/MS scans, and threshold at 1000. A peaklist was created for each analyzed fraction (i.e., gel slice), and individual Mascot (version 2.3.01) searches were performed for each fraction. The data were searched against *Homo sapiens* entries in Uniprot protein database (Feb 2018 release; 20,316 total sequences). Carbamidomethylation of cysteines was set as a fixed modification, and oxidation of methionine was set as a variable modification. Specificity of trypsin digestion was set for cleavage after Lys or Arg, and two missed trypsin cleavage sites were allowed. The mass tolerances in MS and MS/MS were set to 10 ppm and 0.6 Da, respectively, and the instrument setting was specified as "ESITrap." To calculate the false discovery rate (FDR), the search was performed using the "decoy" option in Mascot. The spectral FDR and protein FDR are $0.35 \pm 0.17\%$ and $4.28 \pm 1.99\%$ respectively. A minimum Mascot ion score of 25 and peptide rank 1 was used for automatically accepting all peptide MS/MS spectra. Label free relative protein quantitation (LFQ). Relative protein quantification was performed using spectral count-based LFQ. For each biological sample, data from the individual gel slices were combined. Statistical analysis was performed on all proteins identified with average spectral counts of 2. The spectral count data was normalized by total spectral counts of the targeted protein (PAX8 or PBRM1) in each sample to adjust for differences in overall protein levels among samples. Proteins were considered to have a significant difference in abundance if there was a difference of two fold or greater in normalized spectral counts between experiments and a p value 0.01 using a two-tailed t test. Spectral counts for all proteins and peptides identified are provided in supplementary material.

Bioinformatic and statistical analysis—Protein interaction networks were constructed using Cytoscape 3.4. Briefly, identified proteins were represented as nodes in the network. The size of each node relates to the normalized relative quantification value as defined in "Label free relative protein quantitation (LFQ)": protein node shape was set to "circle"; the length and width (diameter) of the circle were formatted by the continuous mapping function of the software to represent the normalized relative quantification value. Physical protein-protein interaction networks were predicted using STRING v10.0 (http://string.db.org/) with high confidence (parameter value 0.70). Predicted protein-protein interactions were represented as Edges/Links connecting protein nodes; the thickness of each edge represented the statistical significance of the string prediction. Different colors were assigned to protein function complexes, with blue for transcription factors, green for coactivators, and red for corepressors.

Western blot analyses—Approximately 50 μg of protein extracts, together with molecular weight markers, were subjected to 1D SDS-PAGE on 4%–12% gradient gels (Invitrogen). After electrophoresis per manufacturer's manual (Invitrogen), proteins were transferred to PVDF membranes (Millipore) at 35 constant voltage for 1 hour using Invitrogen's semidry blotting apparatus. Western analyses of PVDF membranes utilized established protocols and antibodies for DNMT1 (Abcam #Ab54759), mouse anti-flag

(Sigma cat# F3165-.2MG), rabbit anti-PBRM1 (ABCAM cat# ab86156), rabbit anti c-MYC (Cell signaling cat# 5605), rabbit anti-p27/CDKN1B (Cell signaling Ab cat# 3833) and β-actin (Sigma, #a3854).

Flow cytometry analyses—0.1×10^6 viable cells were harvested at 96 hours post transecfection and stained with 1% propidium iodide (PI) at ambient temperature for 5 minutes. Analysis of forward scatter and side scatter was performed on PI negative cells on Cytomics FC 500 from Beckman coulter.

Murine xenograft and *in vivo* therapy—All experiments were approved by the Cleveland Clinic IACUC protocol number 2464 and followed approved procedures. Male athymic nude mice between 8-12 weeks of age were inoculated sub-cutaneously (right and left flanks) with 2×10^6 RCC cells (Ren-02, patient-derived RCC cell-line, bevacizumab resistant; Diaz-Montero et al., 2016) in 200 μL sterile vehicle. Seven days after inoculation (day 7), mice were initiated on treatment (8 mice/treatment group) with mock treatment - PBS administered subcutaneously 3 days per week, decitabine 0.2 mg/kg administered sub-cutaneously 3 days per week, sunitinib (a multi-kinase [including VEGF pathway] inhibitor that is standard of care for metastatic RCC) 40mg/kg administered by oral gavage daily 5 days per week, or the combination of decitabine 0.1 mg/kg administered subcutaneously 3 days per week after tetrahydrouridine 10 mg/kg administered intraperitoneally. Tumor sizes were measured twice a week using an electronic caliper, and volume estimated using the following equation: volume (mm^3) = long (mm) x wide^2 (mm) / 2. Mice developing tumors over 2,000 mm^3 in size (> 17 mm in diameter) or showing signs of distress or necrosis in any area of the xenograft were euthanized for humanitarian reasons, using CO_2 inhalation followed by cervical dislocation. Tumor was harvested from the euthanized rodents for further analysis. The experiment was terminated when the mice from any experimental group were completely euthanized.

QUANTIFICATION AND STATISTICAL ANALYSIS

Wilcoxon's rank-sum, Mann Whitney U, and t tests were 2-sided and performed at the 0.05 significance level or lower (Bonferroni's corrections were applied for instances of multiple parallel testing). SDs and interquartile ranges (IQR) for each set of measurements were calculated and represented as y axis error bars on each graph. Graph Prism (GraphPad) or SAS statistical software (SAS Institute Inc.) was used to perform statistical analysis including correlation analyses. We did not use formal methods to determine whether the data met assumptions of the statistical approach. The statistical details for each individual experiment can be found in the respective figure legends.

Supplementary Material

Refer to Web version on PubMed Central for supplementary material.

ACKNOWLEDGMENTS

REFERENCES

Acosta JC, Ferrándiz N, Bretones G, Torrano V, Blanco R, Richard C, O'Connell B, Sedivy J, Delgado MD, and Leon J (2008). Myc inhibits p27-induced erythroid differentiation of leukemia cells by repressing erythroid master genes without reversing p27-mediated cell cycle arrest. Mol. Cell. Biol 28, 7286–7295. [PubMed: 18838534]

Agrawal P, Yu K, Salomon AR, and Sedivy JM (2010). Proteomic profiling of Myc-associated proteins. Cell Cycle 9, 4908–4921. [PubMed: 21150319]

Aschauer L, Gruber LN, Pfaller W, Limonciel A, Athersuch TJ, Cavill R, Khan A, Gstraunthaler G, Grillari J, Grillari R, et al. (2013). Delineation of the key aspects in the regulation of epithelial monolayer formation. Mol. Cell. Biol 33, 2535–2550. [PubMed: 23608536]

Barisic D, Stadler MB, Iurlaro M, and Schübeler D (2019). Mammalian ISWI and SWI/SNF selectively mediate binding of distinct transcription factors. Nature 569, 136–140. [PubMed: 30996347]

Barr ML, Jilaveanu LB, Camp RL, Adeniran AJ, Kluger HM, and Shuch B (2015). PAX-8 expression in renal tumours and distant sites: a useful marker of primary and metastatic renal cell carcinoma? J. Clin. Pathol 68, 12–17. [PubMed: 25315900]

Bauer JA, Morrison BH, Grane RW, Jacobs BS, Borden EC, and Lindner DJ (2003). IFN-alpha2b and thalidomide synergistically inhibit tumor-induced angiogenesis. J. Interferon Cytokine Res 23, 3–10. [PubMed: 12639293]

Benusiglio PR, Couvé S, Gilbert-Dussardier B, Deveaux S, Le Jeune H, Da Costa M, Fromont G, Memeteau F, Yacoub M, Coupier I, et al. (2015). A germline mutation in PBRM1 predisposes to renal cell carcinoma. J. Med. Genet 52, 426–430. [PubMed: 25911086]

Bleu M, Gaulis S, Lopes R, Sprouffske K, Apfel V, Holwerda S, Pregnolato M, Yildiz U, Cordo' V, Dost AFM, et al. (2019). PAX8 activates metabolic genes via enhancer elements in Renal Cell Carcinoma. Nat. Commun 10, 3739. [PubMed: 31431624]

Bodmer D, Eleveld MJ, Ligtenberg MJ, Weterman MA, Janssen BA, Smeets DF, de Wit PE, van den Berg A, van den Berg E, Koolen MI, and Geurts van Kessel A (1998). An alternative route for multistep tumorigenesis in a novel case of hereditary renal cell cancer and a t(2;3)(q35;q21) chromosome translocation. Am. J. Hum. Genet 62, 1475–1483. [PubMed: 9585616]

Boualia SK, Gaitan Y, Tremblay M, Sharma R, Cardin J, Kania A, and Bouchard M (2013). A core transcriptional network composed of Pax2/8, Gata3 and Lim1 regulates key players of pro/mesonephros morphogenesis. Dev. Biol 382, 555–566. [PubMed: 23920117]

Bouchard M, Souabni A, Mandler M, Neübuser A, and Busslinger M (2002). Nephric lineage specification by Pax2 and Pax8. Genes Dev. 16, 2958–2970. [PubMed: 12435636]

Brunskill EW, Aronow BJ, Georgas K, Rumballe B, Valerius MT, Aronow J, Kaimal V, Jegga AG, Yu J, Grimmond S, et al. (2008). Atlas of gene expression in the developing kidney at microanatomic resolution. Dev. Cell 15, 781–791. [PubMed: 19000842]

Buisson I, Le Bouffant R, Futel M, Riou JF, and Umbhauer M (2015). Pax8 and Pax2 are specifically required at different steps of Xenopus pronephros development. Dev. Biol 397, 175–190. [PubMed: 25446030]

Cancer Genome Atlas Research Network (2013). Comprehensive molecular characterization of clear cell renal cell carcinoma. Nature 499, 43–49. [PubMed: 23792563]

Carvalho A, Hermanns P, Rodrigues AL, Sousa I, Anselmo J, Bikker H, Cabral R, Pereira-Duarte C, Mota-Vieira L, and Pohlenz J (2013). A new PAX8 mutation causing congenital hypothyroidism in three generations of a family is associated with abnormalities in the urogenital tract. Thyroid 23, 1074–1078. [PubMed: 23647375]

Chowdhury B, Porter EG, Stewart JC, Ferreira CR, Schipma MJ, and Dykhuizen EC (2016). PBRM1 Regulates the Expression ofGenes Involved in Metabolism and Cell Adhesion in Renal Clear Cell Carcinoma. PLoS ONE 11, e0153718. [PubMed: 27100670]

Chronis C, Fiziev P, Papp B, Butz S, Bonora G, Sabri S, Ernst J, and Plath K (2017). Cooperative Binding of Transcription Factors Orchestrates Reprogramming. Cell 163, 442–459.e20.

Cooper SJ, Zou H, Legrand SN, Marlow LA, von Roemeling CA, Radisky DC, Wu KJ, Hempel N, Margulis V, Tun HW, et al. (2010). Loss of type III transforming growth factor-beta receptor

expression is due to methylation silencing of the transcription factor GATA3 in renal cell carcinoma. Oncogene 29, 2905–2915. [PubMed: 20208565]

Dang CV, Kim JW, Gao P, and Yustein J (2008). The interplay between MYC and HIF in cancer. Nat. Rev. Cancer 3, 51–56.

Dannenberg JH, David G, Zhong S, van der Torre J, Wong WH, and Depinho RA (2005). mSin3A corepressor regulates diverse transcriptional networks governing normal and neoplastic growth and survival. Genes Dev. 19, 1581–1595. [PubMed: 15998811]

Dehbi M, and Pelletier J (1996). PAX8-mediated activation of the wt1 tumor suppressor gene. EMBO J. 15, 4297–4306. [PubMed: 8861958]

di Gennaro A, Spadaro O, Baratta MG, De Felice M, and Di Lauro R (2013). Functional analysis of the murine Pax8 promoter reveals autoregulation and the presence of a novel thyroid-specific DNA-binding activity. Thyroid 23, 488–496. [PubMed: 23078112]

Di Palma T, Filippone MG, Pierantoni GM, Fusco A, Soddu S, and Zannini M (2013). Pax8 hascritical role in epithelial cell survival and proliferation. Cell Death Dis. 4, e729. [PubMed: 23868062]

Diaz-Montero CM, Mao FJ, Barnard J, Parker Y, Zamanian-Daryoush M, Pink JJ, Finke JH, Rini BI, and Lindner DJ (2016). MEK inhibition abrogates sunitinib resistance in a renal cell carcinoma patient-derived xenograft model. Br. J. Cancer 115, 920–928. [PubMed: 27560553]

Eberl HC, Spruijt CG, Kelstrup CD, Vermeulen M, and Mann M (2013). A map of general and specialized chromatin readers in mouse tissues generated by label-free interaction proteomics. Mol. Cell 49, 368–378. [PubMed: 23201125]

Ebert T, Bander NH, Finstad CL, Ramsawak RD, and Old LJ (1990). Establishment and characterization of human renal cancer and normal kidney cell lines. Cancer Res. 50, 5531–5536. [PubMed: 2386958]

Eisenberg E, and Levanon EY (2013). Human housekeeping genes, revisited. Trends Genet. 29, 569–574. [PubMed: 23810203]

Ellinger J, Kahl P, Mertens C, Rogenhofer S, Hauser S, Hartmann W, Bastian PJ, Büttner R, Müller SC, and von Ruecker A (2010). Prognostic relevance of global histone H3 lysine 4 (H3K4) methylation in renal cell carcinoma. Int. J. Cancer 127, 2360–2366. [PubMed: 20162570]

Enane FO, Shuen WH, Gu X, Quteba E, Przychodzen B, Makishima H, Bodo J, Ng J, Chee CL, Ba R, et al. (2017a). GATA4 loss of function in liver cancer impedes precursor to hepatocyte transition. J. Clin. Invest 127, 3527–3542. [PubMed: 28758902]

Fraizer GC, Shimamura R, Zhang X, and Saunders GF (1997). PAX8 regulates human WT1 transcription through a novel DNA binding site. J. Biol. Chem 272, 30678–30687. [PubMed: 9388203]

Ge X, Yamamoto S, Tsutsumi S, Midorikawa Y, Ihara S, Wang SM, and Aburatani H (2005). Interpreting expression profiles of cancers by genome-wide survey of breadth of expression in normal tissues. Genomics 36, 127–141.

Green LM, Wagner KJ, Campbell HA, Addison K, and Roberts SG (2009). Dynamic interaction between WT1 and BASP1 in transcriptional regulation during differentiation. Nucleic Acids Res. 37, 431–440. [PubMed: 19050011]

Grote D, Souabni A, Busslinger M, and Bouchard M (2006). Pax2/8-regulated Gata 3 expression is necessary for morphogenesis and guidance of the nephric duct in the developing kidney. Development 133, 53–61. [PubMed: 16319112]

Gu X, Hu Z, Ebrahem Q, Crabb JS, Mahfouz RZ, Radivoyevitch T, Crabb JW, and Saunthararajah Y (2014). Runx1 regulation of Pu.1 corepressor/coactivator exchange identifies specific molecular targets for leukemia differentiation therapy. J. Biol. Chem 239, 14881–14895.

Gu YF, Cohn S, Christie A, McKenzie T, Wolff N, Do QN, Madhuranthakam AJ, Pedrosa I, Wang T, Dey A, et al. (2017). Modeling Renal Cell Carcinoma in Mice: *Bap1* and *Pbrm1* Inactivation DriveTumor Grade. Cancer Discov. 7, 900–917. [PubMed: 28473526]

Gu X, Ebrahem Q, Mahfouz RZ, Hasipek M, Enane F, Radivoyevitch T, Rapin N, Przychodzen B, Hu Z, Balusu R, et al. (2018). Leukemogenic nucleophosmin mutation disrupts the transcription factor hub that regulates granulomonocytic fates. J. Clin. Invest 123, 4260–4279.

Hartley PD, and Madhani HD (2009). Mechanisms that specify promoter nucleosome location and identity. Cell 137, 445–458. [PubMed: 19410542]

Heng DY, Xie W, Regan MM, Harshman LC, Bjarnason GA, Vaishampayan UN, Mackenzie M, Wood L, Donskov F, Tan MH, et al. (2013). External validation and comparison with other models of the International Metastatic Renal-Cell Carcinoma Database Consortium prognostic model: a population-based study. Lancet Oncol. 14, 141–148. [PubMed: 23312463]

Ho TH, Kapur P, Joseph RW, Serie DJ, Eckel-Passow JE, Tong P, Wang J, Castle EP, Stanton ML, Cheville JC, et al. (2016). Loss of histone H3 lysine 36 trimethylation is associated with an increased risk of renal cell carcinoma-specific death. Mod. Pathol 29, 34–42. [PubMed: 26516698]

Holthöfer H, Miettinen A, Paasivuo R, Lehto VP, Linder E, Alfthan O, and Virtanen I (1983). Cellular origin and differentiation of renal carcinomas. A fluorescence microscopic study with kidney-specific antibodies, antiintermediate filament antibodies, and lectins. Lab. Invest 49, 317–326. [PubMed: 6193332]

Hu Z, Gu X, Baraoidan K, Ibanez V, Sharma A, Kadkol S, Munker R, Ackerman S, Nucifora G, and Saunthararajah Y (2011). RUNX1 regulates corepressor interactions of PU.1. Blood 117, 6498–6508. [PubMed: 21518930]

Hu CY, Mohtat D, Yu Y, Ko YA, Shenoy N, Bhattacharya S, Izquierdo MC, Park AS, Giricz O, Vallumsetla N, et al. (2014). Kidney cancer is characterized by aberrant methylation of tissue-specific enhancers that are prognostic for overall survival. Clin. Cancer Res 20, 4349–4360. [PubMed: 24916699]

Huang W, Sherman BT, and Lempicki RA (2009). Systematic and integrative analysis of large gene lists using DAVID bioinformatics resources. Nat. Protoc 4, 44–57. [PubMed: 19131956]

Jiang W, Dulaimi E, Devarajan K, Parsons T, Wang Q, O'Neill R, Solomides C, Peiper SC, Testa JR, Uzzo R, and Yang H (2017). Intratumoral heterogeneity analysis reveals hidden associations between protein expression losses and patient survival in clear cell renal cell carcinoma. Oncotarget 8, 37423–37434. [PubMed: 28445125]

Kadam S, and Emerson BM (2003). Transcriptional specificity of human SWI/SNF BRG1 and BRM chromatin remodeling complexes. Mol. Cell 11, 377–389. [PubMed: 12620226]

Kadam S, McAlpine GS, Phelan ML, Kingston RE, Jones KA, and Emerson BM (2000). Functional selectivity of recombinant mammalian SWI/SNF subunits. Genes Dev. 14, 2441–2451. [PubMed: 11018012]

Kanao K, Mikami S, Mizuno R, Shinojima T, Murai M, and Oya M (2008). Decreased acetylation of histone H3 in renal cell carcinoma: a potential target of histone deacetylase inhibitors. J. Urol 130, 1131–1136.

Kim J, Woo AJ, Chu J, Snow JW, Fujiwara Y, Kim CG, Cantor AB, and Orkin SH (2010). A Myc network accounts for similarities between embryonic stem and cancer cell transcription programs. Cell 143, 313–324. [PubMed: 20946988]

Klingel R, Dippold W, Störkel S, Meyer zum Büschenfelde KH, and Köhler H (1992). Expression of differentiation antigens and growth-related genes in normal kidney, autosomal dominant polycystic kidney disease, and renal cell carcinoma. Am. J. Kidney Dis 19, 22–30. [PubMed: 1739078]

Kojima T, Shimazui T, Horie R, Hinotsu S, Oikawa T, Kawai K, Suzuki H, Meno K, Akaza H, and Uchida K (2010). FOXO1 and TCF7L2 genes involved in metastasis and poor prognosis in clear cell renal cell carcinoma. Genes Chromosomes Cancer 49, 379–389. [PubMed: 20095040]

Lemon B, Inouye C, King DS, and Tjian R (2001). Selectivity of chromatin-remodelling cofactors for ligand-activated transcription. Nature 414, 924–928. [PubMed: 11780067]

Li FP, Decker HJ, Zbar B, Stanton VP Jr., Kovacs G, Seizinger BR, Aburatani H, Sandberg AA, Berg S, Hosoe S, and Brown RS (1993). Clinical and genetic studies of renal cell carcinomas in a family with a constitutional chromosome 3;8 translocation. Genetics of familial renal carcinoma. Ann. Intern. Med 118, 106–111. [PubMed: 8416305]

Li CG, Nyman JE, Braithwaite AW, and Eccles MR (2011). PAX8 promotes tumor cell growth by transcriptionally regulating E2F1 and stabilizing RB protein. Oncogene 30, 4824–4834. [PubMed: 21602887]

Linderson Y, Eberhard D, Malin S, Johansson A, Busslinger M, and Pettersson S (2004). Corecruitment of the Grg4 repressor by PU.1 is critical for Pax5-mediated repression of B-cell-specific genes. EMBO Rep. 5, 291–296. [PubMed: 14993928]

Lindgren D, Eriksson P, Krawczyk K, Nilsson H, Hansson J, Veerla S, Sjölund J, Höglund M, Johansson ME, and Axelson H (2017). Cell-Type-Specific Gene Programs of the Normal Human Nephron Define Kidney Cancer Subtypes. Cell Rep. 20, 1476–1489. [PubMed: 28793269]

Lucas B, Grigo K, Erdmann S, Lausen J, Klein-Hitpass L, and Ryffel GU (2005). HNF4alpha reduces proliferation of kidney cells and affects genes deregulated in renal cell carcinoma. Oncogene 24, 6418–6431. [PubMed: 16007190]

Marr MT 2nd, Isogai Y, Wright KJ, and Tjian R (2006). Coactivator cross-talk specifies transcriptional output. Genes Dev. 20, 1458–1469. [PubMed: 16751183]

McDonald ER 3rd, de Weck A, Schlabach MR, Billy E, Mavrakis KJ, Hoffman GR, Belur D, Castelletti D, Frias E, Gampa K, et al. (2017). Project DRIVE: A Compendium of Cancer Dependencies and Synthetic Lethal Relationships Uncovered by Large-Scale, Deep RNAi Screening. Cell 170, 577–592.e10. [PubMed: 28753431]

Meeus L, Gilbert B, Rydlewski C, Parma J, Roussie AL, Abramowicz M, Vilain C, Christophe D, Costagliola S, and Vassart G (2004). Characterization of a novel loss of function mutation of PAX8 in a familial case of congenital hypothyroidism with in-place, normal-sized thyroid. J. Clin. Endocrinol. Metab 89, 4285–4291. [PubMed: 15356023]

Minardi D, Lucarini G, Filosa A, Milanese G, Zizzi A, Primio RD, Montironi R, and Muzzonigro G (2009). Prognostic role of global DNA-methylation and histone acetylation in pT1a clear cell renal carcinoma in partial nephrectomy specimens. J. Cell. Mol. Med 13 (8B), 2115–2121. [PubMed: 18752633]

Mosashvilli D, Kahl P, Mertens C, Holzapfel S, Rogenhofer S, Hauser S, Büttner R, Von Ruecker A, Müller SC, and Ellinger J (2010). Global histone acetylation levels: prognostic relevance in patients with renal cell carcinoma. Cancer Sci. 101, 2664–2669. [PubMed: 20825416]

Nargund AM, Pham CG, Dong Y, Wang PI, Osmangeyoglu HU, Xie Y, Aras O, Han S, Oyama T, Takeda S, et al. (2017). The SWI/SNF Protein PBRM1 Restrains VHL-Loss-Driven Clear Cell Renal Cell Carcinoma. Cell Rep. 18, 2893–2906. [PubMed: 28329682]

Narlis M, Grote D, Gaitan Y, Boualia SK, and Bouchard M (2007). Pax2 and pax8 regulate branching morphogenesis and nephron differentiation in the developing kidney. J. Am. Soc. Nephrol 18, 1121–1129. [PubMed: 17314325]

Negrotto S, Hu Z, Alcazar O, Ng KP, Triozzi P, Lindner D, Rini B, and Saunthararajah Y (2011). Noncytotoxic differentiation treatment of renal cell cancer. Cancer Res. 71, 1431–1441. [PubMed: 21303982]

Parnell TJ, Huff JT, and Cairns BR (2008). RSC regulates nucleosome positioning at Pol II genes and density at Pol III genes. EMBO J. 27, 100–110. [PubMed: 18059476]

Pawłowski R, Mühl SM, Sulser T, Krek W, Moch H, and Schraml P (2013). Loss of PBRM1 expression is associated with renal cell carcinoma progression. Int. J. Cancer 132, E11–E17. [PubMed: 22949125]

Perissi V, Jepsen K, Glass CK, and Rosenfeld MG (2010). Deconstructing repression: evolving models of co-repressor action. Nat. Rev. Genet 11, 109–123. [PubMed: 20084085]

Ram O, Goren A, Amit I, Shoresh N, Yosef N, Ernst J, Kellis M, Gymrek M, Issner R, Coyne M, et al. (2011). Combinatorial patterning of chromatin regulators uncovered by genome-wide location analysis in human cells. Cell 147, 1628–1639. [PubMed: 22196736]

Ramaswamy S, Nakamura N, Sansal I, Bergeron L, and Sellers WR (2002). A novel mechanism of gene regulation and tumor suppression by the transcription factor FKHR. Cancer Cell 2, 81–91. [PubMed: 12150827]

Ribes D, Fischer E, Calmont A, and Rossert J (2003). Transcriptional control of epithelial differentiation during kidney development. J. Am. Soc. Nephrol 14 (Suppl 1), S9–S15. [PubMed: 12761232]

Rosenfeld MG, Lunyak VV, and Glass CK (2006). Sensors and signals: a coactivator/corepressor/epigenetic code for integrating signal-dependent programs of transcriptional response. Genes Dev. 20, 1405–1428. [PubMed: 16751179]

Saunthararajah Y, Sekeres M, Advani A, Mahfouz R, Durkin L, Radivoyevitch T, Englehaupt R, Juersivich J, Cooper K, Husseinzadeh H, et al. (2015). Evaluation of noncytotoxic DNMT1-depleting therapy in patients with myelodysplastic syndromes. J. Clin. Invest 125, 1043–1055. [PubMed: 25621498]

Sen P, Luo J, Hada A, Hailu SG, Dechassa ML, Persinger J, Brahma S, Paul S, Ranish J, and Bartholomew B (2017). Loss of Snf5 Induces Formation of an Aberrant SWI/SNF Complex. Cell Rep. 18, 2135–2147. [PubMed: 28249160]

Shain AH, and Pollack JR (2013). The spectrum of SWI/SNF mutations, ubiquitous in human cancers. PLoS ONE 8, e55119. [PubMed: 23355908]

Shuib S, Wei W, Sur H, Morris MR, McMullan D, Rattenberry E, Meyer E, Maxwell PH, Kishida T, Yao M, et al. (2011). Copy number profiling in von Hippel-Lindau disease renal cell carcinoma. Genes Chromosomes Cancer 50, 479–488. [PubMed: 21456047]

Sikorski TW, Joo YJ, Ficarro SB, Askenazi M, Buratowski S, and Marto JA (2012). Proteomic analysis demonstrates activator- and chromatin-specific recruitment to promoters. J. Biol. Chem 287, 35397–35408. [PubMed: 22902623]

Söderström M, Vo A, Heinzel T, Lavinsky RM, Yang WM, Seto E, Peterson DA, Rosenfeld MG, and Glass CK (1997). Differential effects of nuclear receptor corepressor (N-CoR) expression levels on retinoic acid receptor-mediated repression support the existence of dynamically regulated corepressor complexes. Mol. Endocrinol 11, 682–692. [PubMed: 9171232]

Tsherniak A, Vazquez F, Montgomery PG, Weir BA, Kryukov G, Cowley GS, Gill S, Harrington WF, Pantel S, Krill-Burger JM, et al. (2017). Defining a Cancer Dependency Map. Cell 170, 564–576.e16. [PubMed: 28753430]

Tun HW, Marlow LA, von Roemeling CA, Cooper SJ, Kreinest P, Wu K, Luxon BA, Sinha M, Anastasiadis PZ, and Copland JA (2010). Pathway signature and cellular differentiation in clear cell renal cell carcinoma. PLoS ONE 5, e10696. [PubMed: 20502531]

Velcheti V, Radivoyevitch T, and Saunthararajah Y (2017). Higher-Level Pathway Objectives of Epigenetic Therapy: A Solution to the p53 Problem in Cancer. Am. Soc. Clin. Oncol. Educ. Book 37, 812–824. [PubMed: 28561650]

Velcheti V, Schrump D, and Saunthararajah Y (2018). Ultimate Precision: Targeting Cancer but Not Normal Self-replication. Am. Soc. Clin. Oncol. Educ. Book 38, 950–963. [PubMed: 30231326]

Wang Z, Zang C, Cui K, Schones DE, Barski A, Peng W, and Zhao K (2009). Genome-wide mapping of HATs and HDACs reveals distinct functions in active and inactive genes. Cell 138, 1019–1031. [PubMed: 19698979]

Wu H, Xiao Y, Zhang S, Ji S, Wei L, Fan F, Geng J, Tian J, Sun X, Qin F, et al. (2013). The Ets transcription factor GABP is a component of the hippo pathway essential for growth and antioxidant defense. Cell Rep. 3, 1663–1677. [PubMed: 23684612]

Yang S, Cho YS, Chennathukuzhi VM, Underkoffler LA, Loomes K, and Hecht NB (2004). Translin-associated factor X is post-transcriptionally regulated by its partner protein TB-RBP, and both are essential for normal cell proliferation. J. Biol. Chem 279, 12605–12614. [PubMed: 14711818]

Zamir I, Zhang J, and Lazar MA (1997). Stoichiometric and steric principles governing repression by nuclear hormone receptors. Genes Dev. 11, 835–846. [PubMed: 9106656]

Highlights

- PBRM1 is a coactivator recruited by transcription factors to activate target genes

- PBRM1 is genetically inactivated in almost all clear cell renal cell cancers (RCCs)

- The transcription factor PAX8 uses PBRM1 to drive proximal tubule epithelial fates

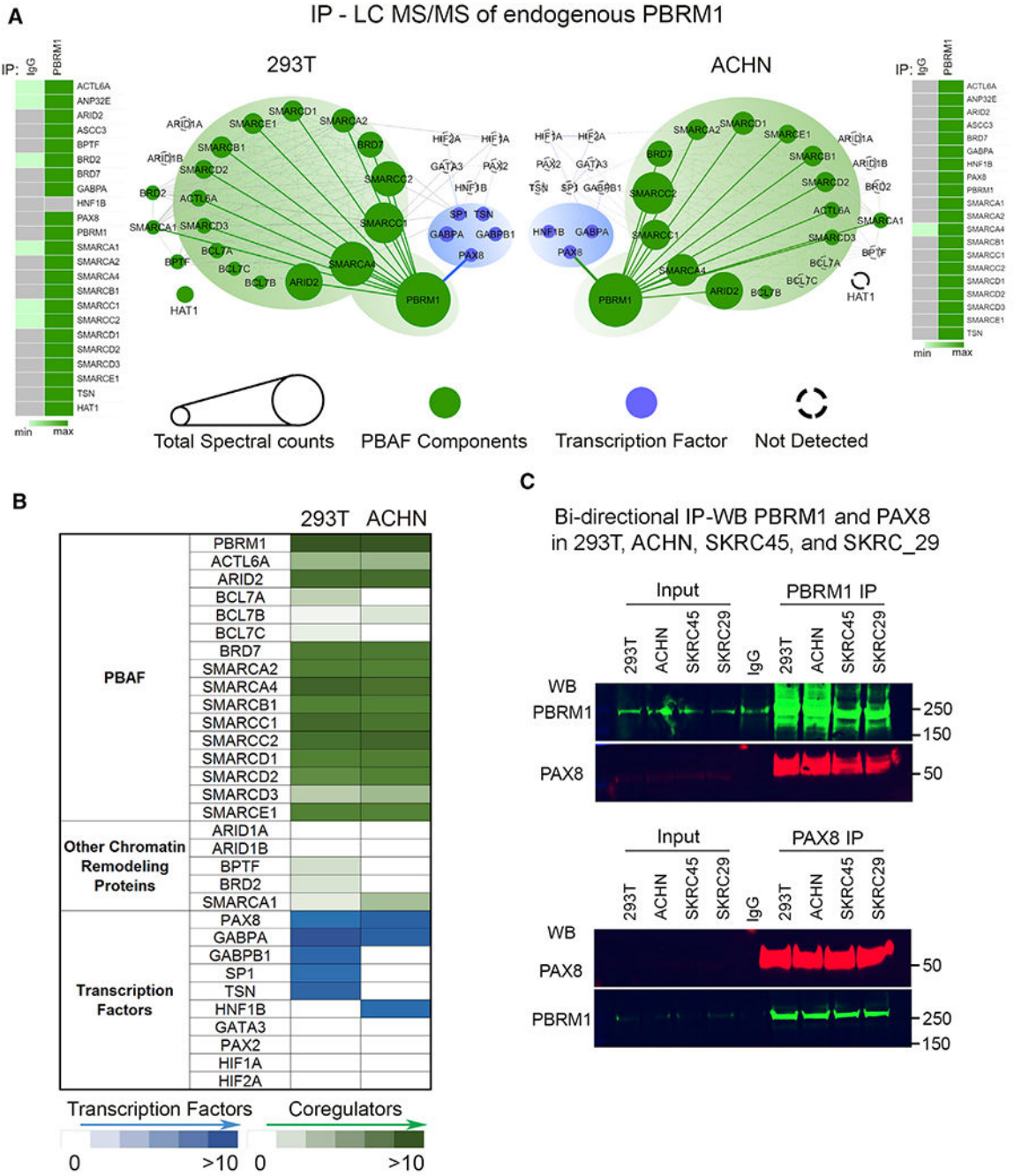- Restoring PBRM1, or inhibiting opposing corepressors, freed RCC cells to such fates

**Figure 1. The PBRM1 protein interactome in kidney lineage cells**

(A) Endogenous PBRM1 was immunoprecipitated (IP) from human embryonic kidney cells (HEK293, left) and RCC cells (ACHN, right), and co-purified proteins were analyzed by LCMS/MS. Shown are identified coactivator (CoA) components and transcription factors. Circle size indicates abundance of protein in the interactome. A minimum Mascot ion score of 25 and peptide rank 1 were used for automatically accepting all peptide MS/MS spectra. The most enriched functional group was "ATPase chromatin remodeling complex" (p value Bonferroni-corrected 1.42×10^{-27}). The STRING database system was used to construct

the protein-protein interaction network with a parameter STRONG score >0.4. Detection, quantification, Gene Ontology (GO), and STRING data for these and other proteins are in Table S1. Heatmap shows quantification versus IP with immunoglobulin G (IgG) isotype control.

(B) Heatmap summary of the data shown in (A).

(C) Bi-directional IP-western blots in 293T and three RCC cell lines confirmed the interaction between PBRM1 and PAX8. The RCC cell lines used were ACHN, SKRC45, and SKRC29.
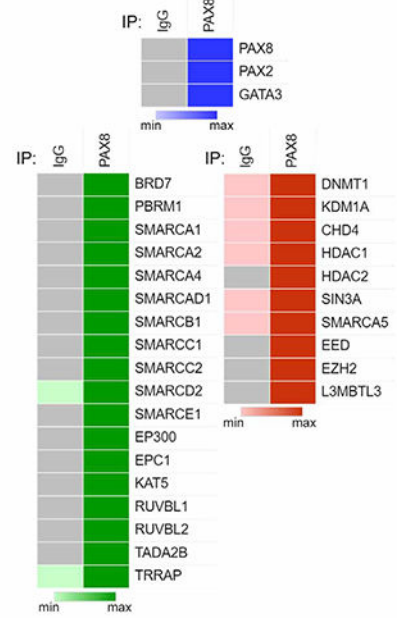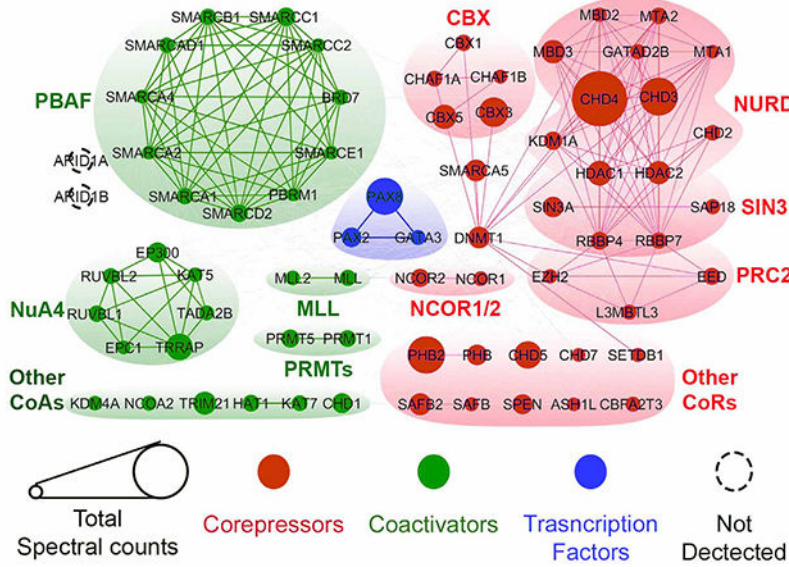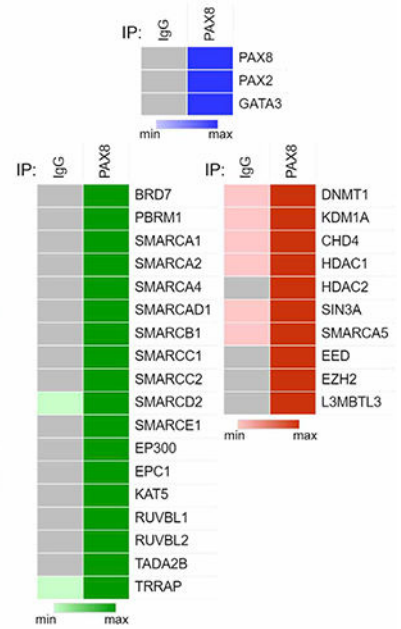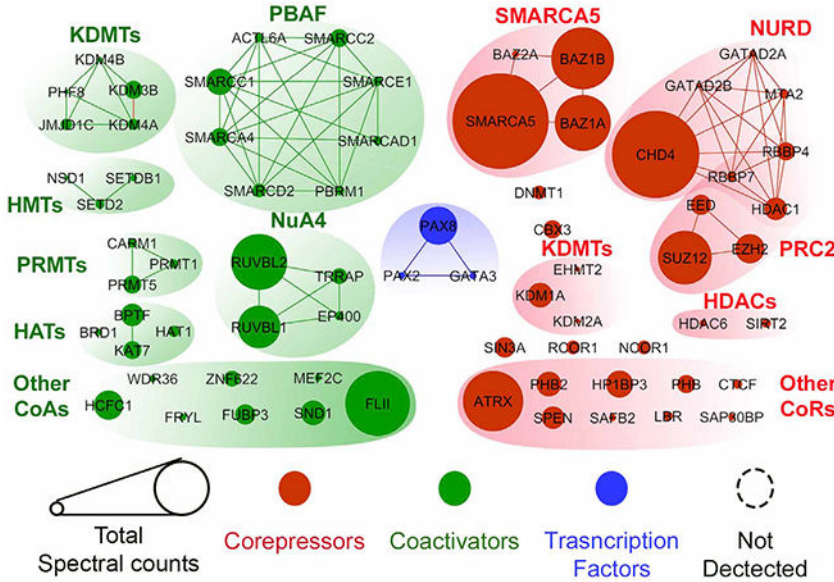
Figure 2. Composition of the PAX8 master transcription factor hub in RCC cells
(A) Endogenous PAX8 was IP from PBRM1-deficient RCC cells (SKRC-45 with deletion of a *PBRM1* allele), and coregulator interactions were analyzed by LCMS/MS. A minimum Mascot ion score of 25 and peptide rank 1 were used for automatically accepting all peptide MS/MS spectra. By GO analyses, the most enriched protein functional groups were the NURD and CBX corepressor(CoR) complexes (p value Bonferroni corrected 3.47×10^{-29}). STRING was used to construct the protein-protein interaction network with a STRONG score >0.4. Circle size indicates abundance of protein in the interactome.

Detection, quantification data, GO, and STRING analyses data are in Table S2. Heatmap shows quantification versus IP with IgG isotype control.

(B) Endogenous PAX8 was IP from PBRM1-deficient RCC cells (ACHN with mutation of a *PBRM1* allele) and coregulator interactions analyzed by LCMS/MS. Analyses as described for (A).
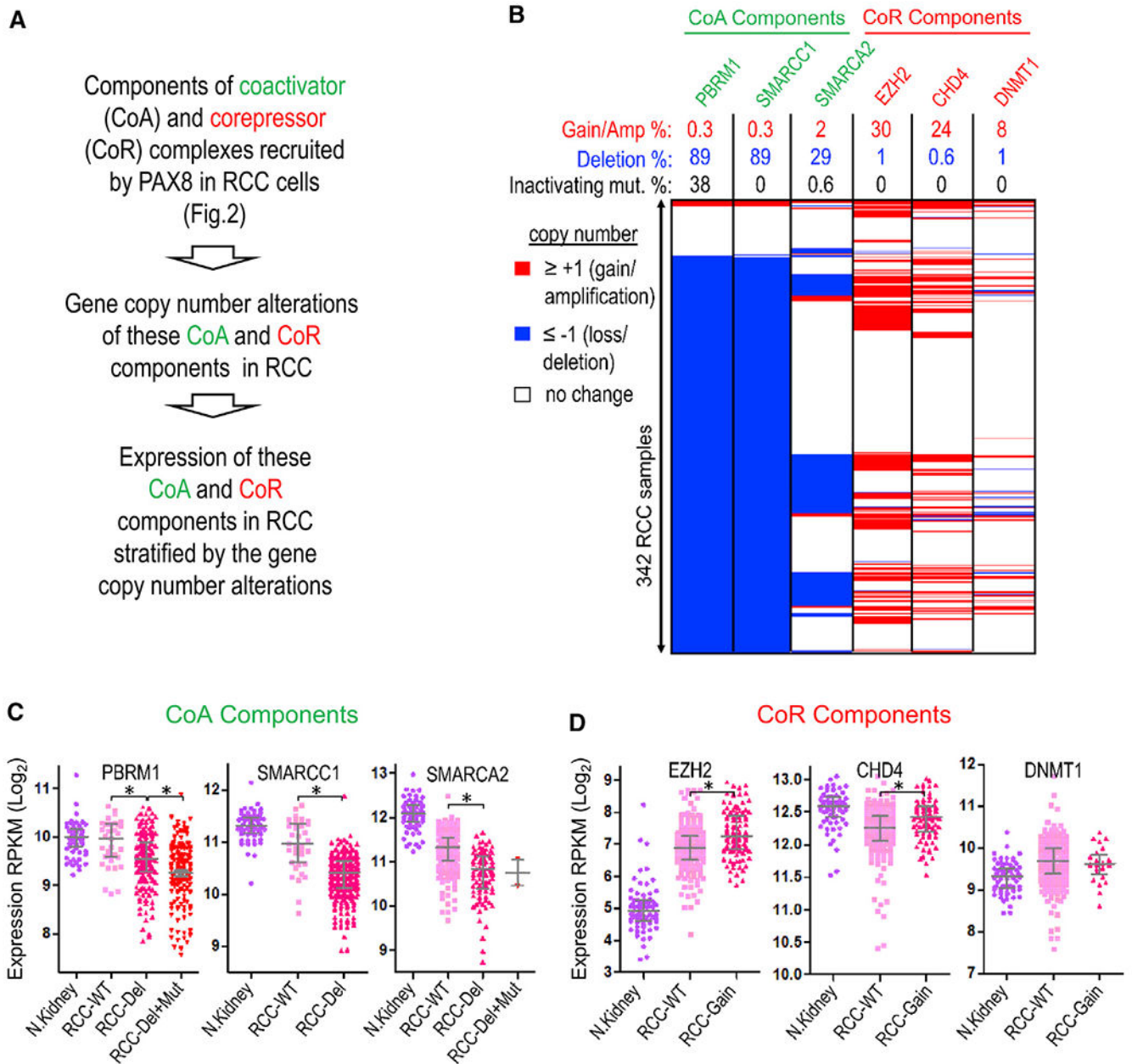
Figure 3. Components of the PBRM1/PBAF CoA recruited by PAX8 are recurrently deleted/mutated in RCC, while druggable CoRs recruited by PAX8 are recurrently amplified

(A) The analysis approach.

(B) Copy numbers of genes for components of the PBAF CoA and for druggable CoR components recruited by PAX8. Gistic thresholded copy-number data from TCGA (n = 342).

(C) The copy-number alterations (predominantly deletions) and inactivating mutations to genes for PBAF CoA components impact their expression accordingly. Gene expression in normal kidney (NKid) and RCCs stratified by recurrent deletions and mutations of CoA

genes (RNA sequencing [RNA-seq] TCGA, NKid cortex n = 72, RCC n = 342). Median ± interquartile range (IQR). *p < 0.001, two-sided Mann-Whitney test.

(D) The copy-number alterations to genes for druggable CoR components (predominantly gains/amplifications) impact their expression accordingly. Gene expression in NKid and RCCs stratified by recurrent gains/amplifications of CoR genes (RNA-seq TCGA, NKid cortex n = 72, RCC n = 342). Median ± IQR. *p < 0.001, two-sided Mann-Whitney test.
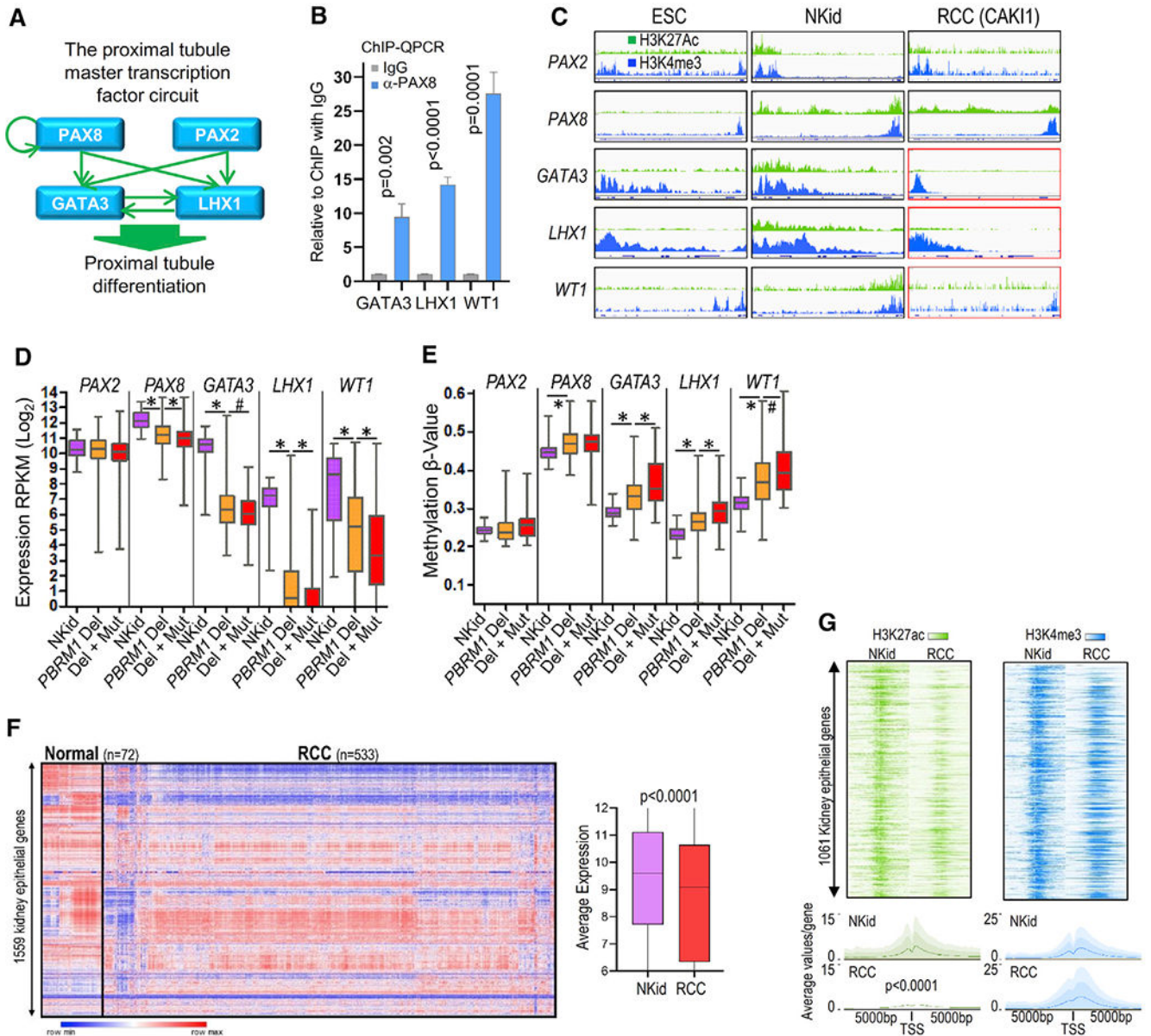
Figure 4. The core transcription factor circuit that drives proximal tubular fates is interrupted between PAX8/PAX2 and GATA3/LHX1/WT1 in RCC, specifically by loss of H3K27ac

(A) The proximal tubule core transcription factor circuit (Boualia et al., 2013).

(B) PAX8 localizes at regulatory regions of *GATA3*, *LHX1*, and *WT1*. Chromatin IP (ChIP)-qRT-PCR analyses using α-PAX8 and IgG isotype control; primers amplified proximal promoter regions. Mean + SD for three biological replicates. Two-sided unpaired t test.

(C) Selective loss in RCC (CAKI1)of H3K27Ac but not H3K4me3 at key PAX8 transcription factor target-genes (*GATA3*, *LHX1*, and *WT1*; red boxes). NKid, normal kidney. H3K27Ac and H3K4me3 public ChIP-seq data (Encode and E-MTAB-7812; Bleu et al., 2019).

(D) *GATA3/LHX1/WT1* are least activated in RCCs with biallelic *PBRM1* inactivation (Del+Mut, deletion and mutation). NKid n = 72, RCC with *PBRM1* Del n = 256, RCC with

PBRM1 Del+Mut n = 180 (TCGA, RNA-seq). Boxplot = median ± IQR, whiskers = range. *p < 0.001, #p < 0.05, two-sided Mann-Whitney test.

(E) *GATA3*/*LHX1*/*WT1* CpG methylation is greatest in RCCs with *PBRM1* Del+Mut. CpG numbers at each gene: *PAX2*, 49; *PAX8*, 16; *GATA3*, 28; *LHX1*, 31; and *WT1*, 46. NKid n = 160, RCC with *PBRM1* Del n = 74, RCC with *PBRM1* Del+Mut n = 64 (TCGA, 450K Illumina array).

(F) >1,000 proximal tubule genes (kidney epithelial genes) are consistently suppressed in RCCs versus NKid. Genes (Table S3) identified from kidney development and normal tissues gene expression databases. Two-sided unpaired t test for average expression/gene NKid versus RCCs.

(G) H3K27Ac but not H3K4me3 loss at repressed proximal tubule genes (F); ChIP-seq per (C). Two-sided unpaired t test, average ChIP-seq values/gene.
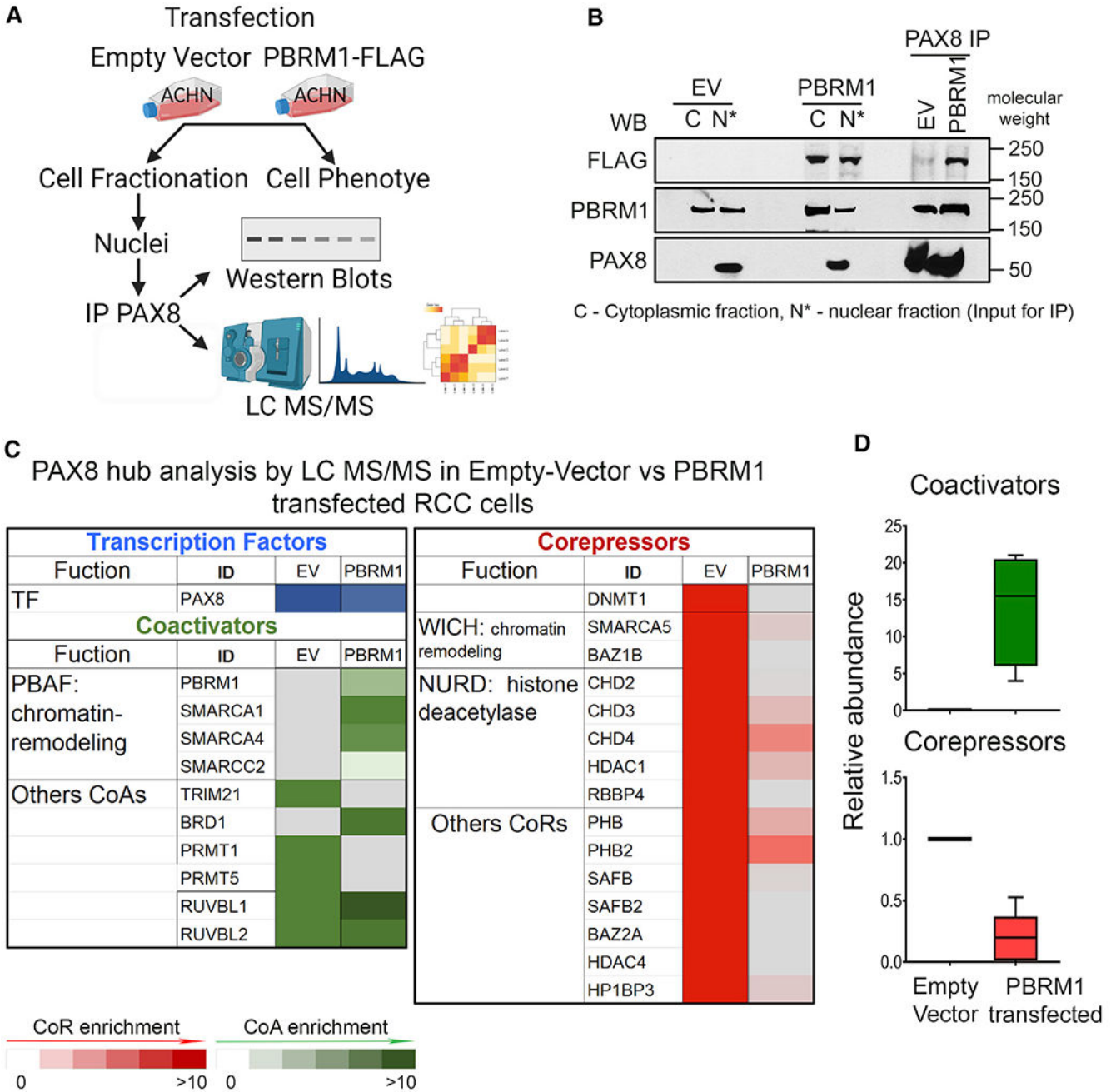
Figure 5. PBRM1 restoration into *PBRM1*-mutated RCC cells shifted coregulator content of the PAX8 hub to CoAs

(A) The experimental approach.

(B) Western blot and IP-western blot analyses of empty vector versus FLAG-PBRM1 transfected RCC (ACHN) cells. PAX8 versus IgG control IP was performed in lysates from empty vector versus PBRM1-FLAG transfected cells 48 h after transfection.

(C) Heatmaps to indicate amounts of coregulators in the PAX8 interactome in empty vector versus FLAG-PBRM1 transfected cells. PAX8 was IP and proteins analyzed by LCMS/MS. Analyses were 48 h after transfection. A minimum Mascot ion score of 25 and peptide

rank 1 were used for automatically accepting all peptide MS/MS spectra. STRING was used to construct the protein-protein interaction network with a STRONG score >0.4. Circle size indicates abundance of protein in the interactome. Detection, quantification, GO, and STRING analyses data are in Table S6.

(D) Relative abundances of CoA and CoR complexes with empty vector versus PBRM1 transfection. The individual proteins constituting CoA and CoR are listed in (A). Median ± IQR. Values analyzed are tabulated in Table S6.
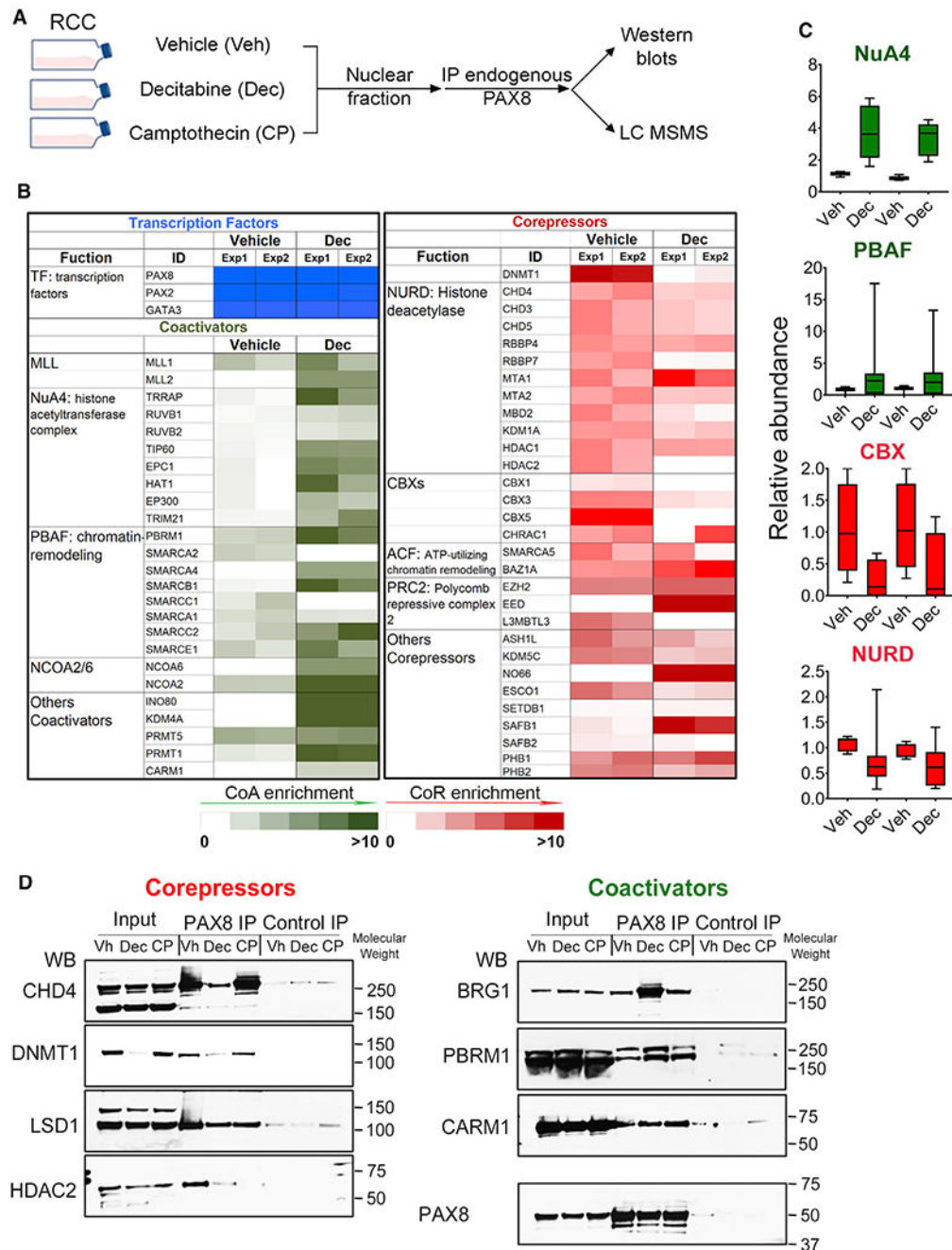
Figure 6. Depletion of the CoR DNMT1 by decitabine (Dec) produced a net shift toward CoAs in the PAX8 hub

(A) The experimental approach.

(B) Heatmaps compare amounts of coregulators in the endogenous PAX8 interactome in vehicle versus Dec-treated RCC cells (SKRC-45). LCMS/MS analyses of proteins pulled down by PAX8 IP. Vehicle or Dec 0.5 μM added on days 1 and 2 and analyses done on day 3. A minimum Mascot ion score of 25 and peptide rank 1 were used for automatically accepting all peptide MS/MS spectra. STRING was used to construct the protein-protein interaction network with a STRONG score >0.4. Circle size indicates abundance of protein

in the interactome. Detection, quantification data, GO, and STRING analyses data are in Table S7.

(C) Relative abundances of specific CoA (green) and CoR (red) complexes with vehicle versus Dec treatment. The individual proteins constituting each complex are listed in (B). Median ± IQR. Values analyzed are tabulated in Table S7.

(D) Western blot and IP-western blot analysis of the PAX8 protein hub in vehicle versus Dec-treated RCC cells. PAX8 versus IgG control IP in lysates from vehicle, Dec, and camptothecin 10 μM (CP, as conventional chemotherapy control) treated RCC (SKRC-45) cells.
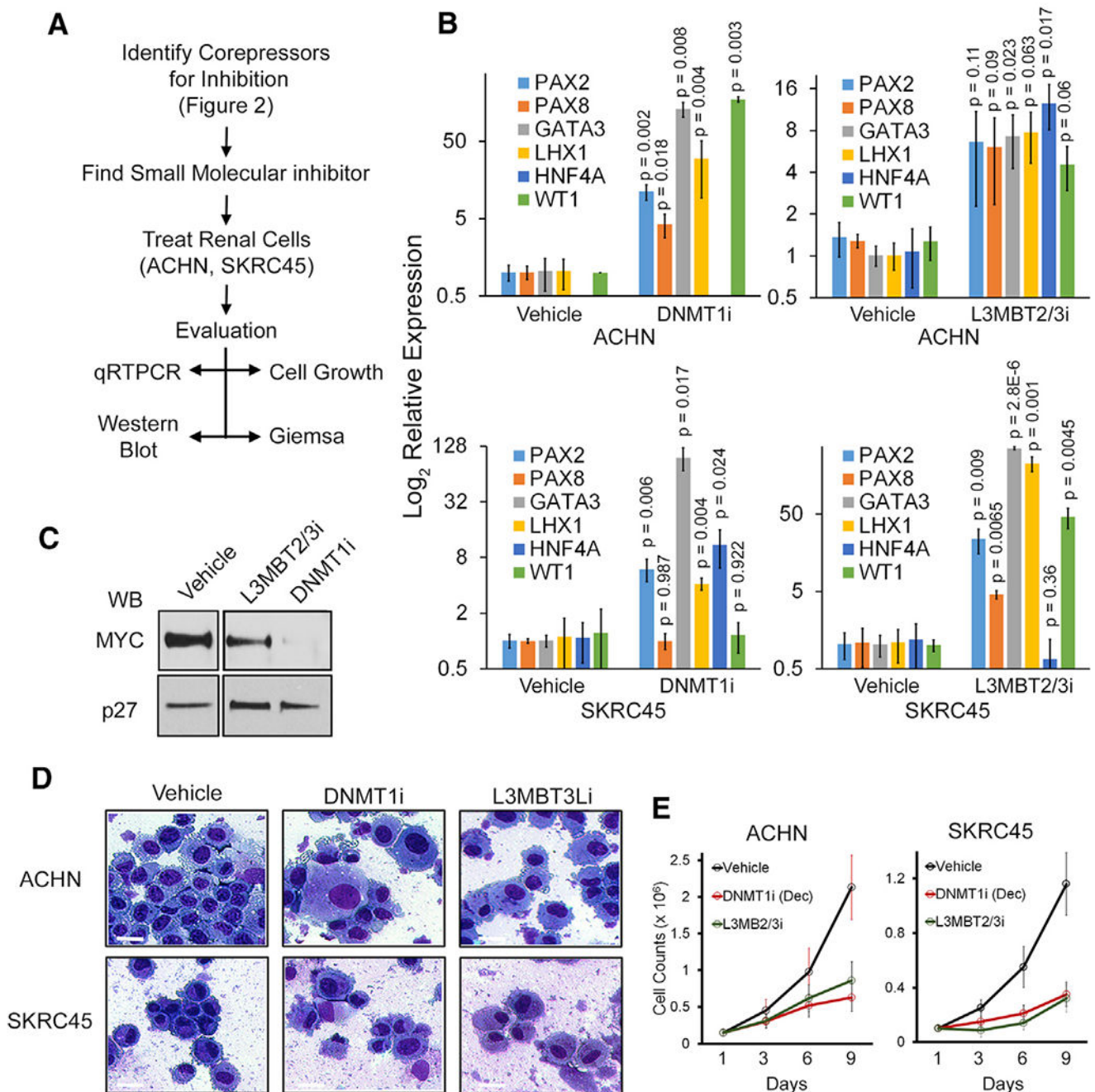
Figure 7. Depletion or inhibition of CoRs in RCC cells activated key PAX8 target genes and terminal epithelial fates

(A) The experimental approach.

(B) GATA3, LHX1, WT1, and HNF4A expression in RCC cells treated with Dec to deplete DNMT1 or UNC1215 to inhibit L3MBTL3. Dec 0.5 μM or UNC1215 1.0 μM added days 1, 2, and 3 each week to RCC cells ACHN and SKRC45. Gene expression by qRT-PCR relative to vehicle-treated control. Plotted are means ± SD for three independent experiments, *p < 0.01, two-sided t test drug versus vehicle.

(C) Western blot for MYC (master regulator of proliferation) and p27/CDKN1B (mediates cell-cycle exits by differentiation). Lanes were run on the same gel but were non-contiguous as indicated.

(D) Giemsa-stained cytospin preparations of cells harvested on day 5. Scale bar (white line), 12.5 μM; magnification, 400×.

(E) Cell counts by automated counter. Plotted are means ± SD from three independent experiments.

KEY RESOURCES TABLE

REAGENT or RESOURCE	SOURCE	IDENTIFIER
Antibodies		
normal mouse IgG	SCBT	sc-2025, RRID: AB_737182
Mouse anti-PAX8	SCBT	sc-81353, RRID: AB_1127048
Rabbit anti-PBRM1	Bethyl Lab	A301-590A, RRID: 1078793
Rabbit anti-PBRM1	Abcam	ab86156, RRID: AB_1925300
Mouse anti-DNMT1	Abcam	Ab54759, RRID: AB_941327
Rabbit anti c-MYC	Cell signaling	5605, RRID: AB_1903938
Mouse anti-flag	Sigma	F3165-.2MG, RRID: AB_259529
Rabbit anti-p27/CDKN1B	Cell signaling	3686, RRID: AB_2077850
Bacterial and virus strains		
3x-p-Flag-CMV4	Cyagen Vectorbuilder	N/A
Biological samples		
Patient-derived xenografts (PDX)	The Ren-02 primary human aRCC cell line was established from a patient-derived primary clear cell renal carcinoma with bevacizumab resistance	N/A
Chemicals, peptides, and recombinant proteins		
Decitabine	Tocris	2624
Tetrahydrouridine	Ash Stevens, Detroit, MI	Custom made
L3MBT2/3L inhibitor	Structural Genomics Consortium	UNC1215
Protease Inhibitor Cocktail	Sigma	P8340
Phosphatase Inhibitor Cocktail 2	Sigma	P5726-5ML
Phosphatase Inhibitor Cocktail 3	Sigma	P0044-5ML
Dimethyl pimelimidate dihydrochloride	Sigma	D8388-1G
N,N,N′,N′-Tetramethylethylenediamine	Sigma	T9281-25ML
Iodoacetamide	Sigma	I1149-5G
Critical commercial assays		
SYBR Advantage qPCR Premix	Clontech	639676
NucleoSpin® RNA	Clontech	740984.5
iScript cDNA synthesis Kit	BioRad	1708891
ChIP DNA Purification Kit	Active Motif	58002
Deposited data		
Protein Identification	ProteomeXchange Consortium (http://proteomecentral.proteomexchange.org)	PXD020544
Experimental models: Cell lines		
ACHN	ATCC	CRL-1611
SKRC45	Gift from Dr N.H. Banker	N/A
SKRC29	Gift from Dr N.H. Banker	N/A
Experimental models: Organisms/strains		

REAGENT or RESOURCE	SOURCE	IDENTIFIER
Mouse Model	Jackson Laboratories	Outbred homozygous nude ($Foxn1^{nu}$/$Foxn1^{nu}$)
Oligonucleotides		
Primers for RT-qPCR and CHIP-qPCR, see Table S8		N/A
Software and algorithms		
Mascot Daemon version 2.3.2	Matrix Science	N/A
Nuance version 3.0.2 software	PerknElmer, Inc	N/A
Cytoscape 3.4	Cytoscape (OpenSource)	https://cytoscape.org
STRING v10.0	STRING	https://string-db.org
Graph Prism	GraphPad	GraphPadv8
SAS statistical software	SAS Institute Inc.	SASv8
FlowJo v10.7	FlowJo	https://www.flowjo.com/solutions/flowjo/downloads
Xcalibur 4.1	Thermo Fisher Scientific	https://assets.thermofisher.com/TFS-Assets/CMD/manuals/man-xcali-97928-xcalibur-41-quan-start-manxcali97928-en.pdf
TraceFinder 4.1	Thermo Fisher Scientific	https://www.thermofisher.com/us/en/home/industrial/mass-spectrometry/liquid-chromatography-mass-spectrometry-lc-ms/lc-ms-software/lc-ms-data-acquisition-software/tracefinder-software.html